CIRP Annals - Manufacturing Technology 62 (2013) 823–846

Contents lists available at SciVerse ScienceDirect

CIRP Annals - Manufacturing Technology

journal homepage: http://ees.elsevier.com/cirp/default.asp

Manufacturing and measurement of freeform optics

F.Z. Fang (1)[a,*], X.D. Zhang [a], A. Weckenmann (1)[b], G.X. Zhang (1)[a], C. Evans (1)[c]

[a] State Key Laboratory of Precision Measuring Technology and Instruments, Centre of MicroNano Manufacturing Technology – MNMT, Tianjin University, 300072, China
[b] Chair Quality Management and Manufacturing Metrology, University Erlangen-Nuremberg, Germany
[c] University of North Carolina at Charlotte, USA

ARTICLE INFO

Keywords:
Freeform optics
Manufacturing
Measurement

ABSTRACT

Freeform optics is the next-generation of modern optics, bringing advantages of excellent optical performance and system integration. It finds wide applications in various fields, such as new energy, illumination, aerospace and biomedical engineering. The manufacturing of freeform optics is an integrated technology involving optical design, machining, moulding, measurement and characterization. This paper surveys the current application status and research on major technologies in details.

1. Introduction

Freeform surfaces can be defined as surfaces with no axis of rotational invariance (within or beyond the part). Freeform surfaces may appear to have arbitrary shape, and regular or irregular surface structures [52,73,98]. Freeform optics offers new opportunities to optical designers and new challenges for optics manufacturing and measurement. Freeform optics has broad application prospects in various areas, such as green energy, aerospace, illumination, and biomedical engineering. Comparing to traditional optical components, freeform optics has the following features [5,103,191].

- Increased range of manufacturable surfaces, giving optical designers more flexibility and scope for innovation.
- Enhancing the optical system performance to the maximum extent. For instance, freeform optics enable optical performance otherwise impossible, such as simultaneously correcting aberrations, increasing depth of field and expanding field of view.
- Simplifying system structure with fewer surfaces, lower mass, lower cost, smaller package-size and reduced stray-light.
- Realizing system integration easily, and reducing the difficulty in assembly. For example, multiple optical surfaces can be made on one freeform element.

Aspheric optics can be considered a special case of freeform optics with an axis of rotational invariance. Conventionally, an aspheric surface has an axis, while freeform surfaces do not. Fig. 1(a) for example shows an objective lens from Schneider Optics where the application of an aspheric led to half the size and weight and increased image quality [80]. Freeform optics may perform better. Fig. 1(b) shows a lens from Olympus Corporation folded into one piece to implement the optical function that previously needed many components.

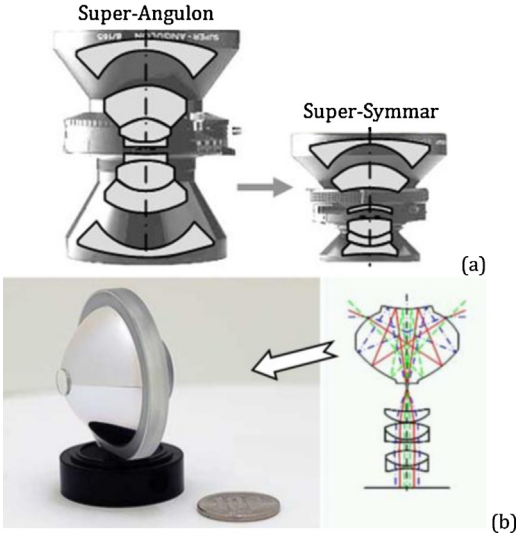

Fig. 1. Examples of aspheric and freeform elements.

Freeform surfaces have been defined in a variety of ways [35,42]. Here we note that one useful classification (given below) satisfies the requirement that there is no axis.

- Continuous smooth surfaces modelled using a mathematic formula and CAD software. Fig. 2(a) shows an example of spiral mirrors applied to the femto-second (fs) laser scanning [232].
- Discontinuous surfaces include steps or facets, which need the truncated functions to describe them. A Fresnel lens (Fig. 2(b)) is a good example often used for lighting optics.
- Structured surfaces, which are the arrays of structure for specific function, therefore called functional surfaces. Fig. 2(c) shows an array of pyramids for the retroreflective application.

* Corresponding author.
E-mail address: fzfang@gmail.com (F.Z. Fang).

0007-8506/$ – see front matter © 2013 CIRP.
http://dx.doi.org/10.1016/j.cirp.2013.05.003

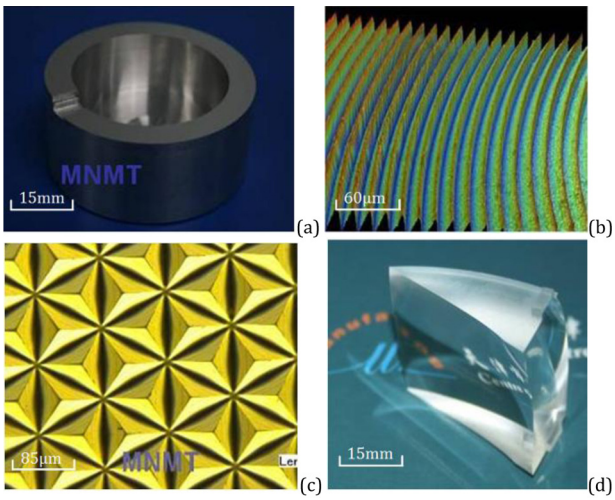

Fig. 2. Examples of freeform optics.

Fig. 3. Polaroid SX-70 camera [181].

- Multiple surfaces on a single substrate, i.e., an integrated lens, containing several optical surfaces, which is a continuous surfaces. Optical freeform prisms are currently the key element of head mounted display (HMD), as shown in Fig. 2(d), consisting of three freeform surfaces [32].

The first successful commercial freeform optical application is often thought in the Polaroid SX-70 folding Single Lens Reflex camera in 1972, as shown in Fig. 3. It is a foldable design and the off-axis viewing system required two freeform lenses to provide well corrected aberrations [181,198]. However, the design concept of asymmetrical optics already exists as early as 1959, when Kanolt et al. designed a multi-focus optical system using *XY* polynomial progressive surfaces [108]. A literature survey of freeform optics from 2000 to date shows that research into freeform optics is dramatically increasing, with most effort related to optical design. Research into machining process and material science is also growing.

The process chain for manufacturing freeform optics, includes design, machining, moulding, metrology and evaluation [224]. Moulding is the main process for mass production (Fig. 4). Metrology includes surface measurements by tactile and by optical methods, as well as the measurement of optical performance. This paper addresses the process chain and typical applications of freeform optics.

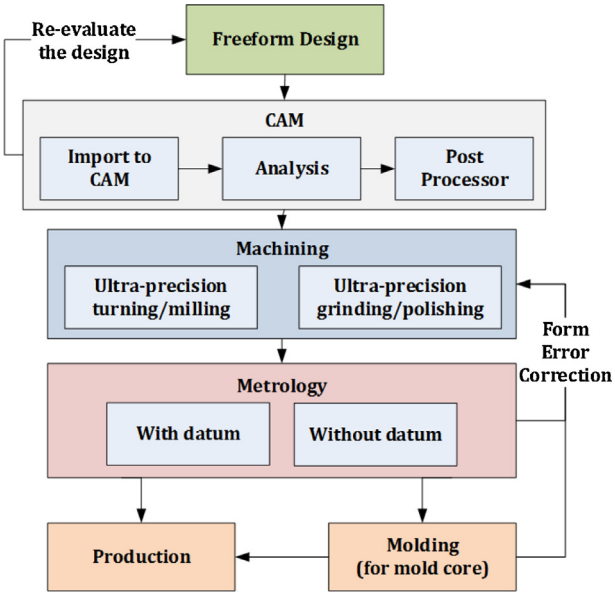

Fig. 4. Manufacture process chain of freeform optics.

2. Applications

There are numerous applications of freeform optics in reflective, refractive, and diffractive optical systems [36,120]. They can be categorized into several areas, such as high-performance imaging, illumination, concentration and other applications.

2.1. Imaging application

Freeform optics used in imaging systems, are designed to improve the optical performance by eliminating the optical aberrations, increasing the depth of field and expanding the field of view. Simultaneously, optical freeforms provide opportunities in realizing system integration and reducing the system size. Moreover, freeform optics can fulfil the special imaging tasks which traditional optics cannot [165,189].

The fields of astronomy and gravitational science have presented significant precision engineering challenges [204]. Freeform optics is adopted to improve the performance of optical systems. Paolo et al. proposed a new layout for an anamorphic collimator based onto two freeform cylinder surfaces, giving diffraction limited images. This collimator can be used to achieve a high resolution spectrograph for large telescopes and an interferometer cavity to test large plano optics [207]. Submillimetre astronomy (at wavelengths of 200 μm–1 mm) is most sensitive to very cold gas and dust. SCUBA-2 (Fig. 5), is composed of nine aluminium freeform mirrors and can inspect large areas of sky up to 1000 times faster than the original SCUBA camera. Scuba 2 also has much larger field-of-view and sky-background limited sensitivity [6,190].

Dowski and Cathey designed cubic phase plates to be used in incoherent hybrid imaging system, which effectively improves the depth of field in microscopes [46]. Sherif et al. also used the idea of

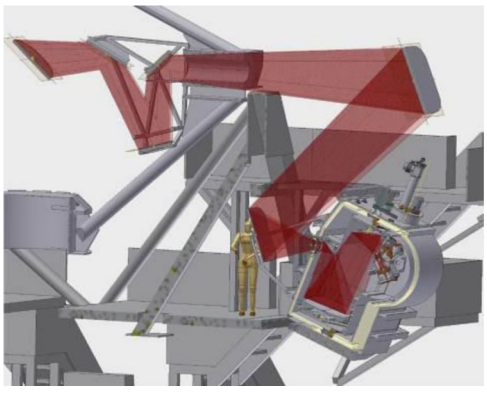

Fig. 5. 3D CAD representation of the SCUBA-2.

Fig. 6. Left image is from a flat driver-side mirror, and right one is from a freeform mirror [165].

wavefront coding to design a log phase plate, which also improves the depth of field, and allows larger defocus [202]. The cubic phase plate was also used in 3D imaging system by Marks et al. [145].

Hicks et al. used the freeform reflector as a driver-side mirror for an automobile that gives a field of view up to 45° so that the mirror has no blind spot and minimal distortion [83]. Fig. 6 shows the visual performance. Another approach to extending the field of view uses a lens array. A compound eye, an aspheric lens array based on a planar or curved substrate, offers a multi aperture imaging. The compound eye on a curved substrate is promising for wide-field-of-view image and parallel image processing, enabling high-speed object tracking [119]. A compound eye on a planar substrate can implement the super-resolution imaging as well as reduce the length of imaging lens greatly. Fraunhofer Institute for Production Technology (IPT) in Germany used a compound eye to design a planar imaging system only 1.4 mm thick (Fig. 7) which is intended to be applied to bank cards for identifying cardholders via image analysis [25,48]. Tanida et al. used compound eyes to design the TOMBO small imaging system, which can be applied in fingerprint recognition [85]. Again there is a theme of structural compactness, increased field of view, and so on.

Panoramic images are the special application of wide-field-of-view systems, where complex catadioptric components may be used. A single conic mirror increases the field, but with increased radial distortion. A freeform mirror solves this problem and yields a cylindrical projection without digital unwrapping, as shown in Fig. 8 [82]. The panoramic annular lens (PAL) is also widely used, which consists of a single piece lens to produce the annular image of the entire 360°. Ma et al. proposed a freeform varifocal PAL design to achieve the zooming effect through a rotation of PAL around optical axis while not moving lenses [137]. Fig. 9 shows the model of this freeform varifocal PAL.

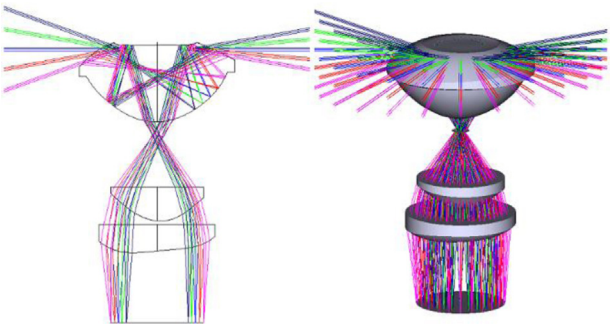

Fig. 9. 2D model (left) and 3D model (right) of freeform varifocal PAL [137].

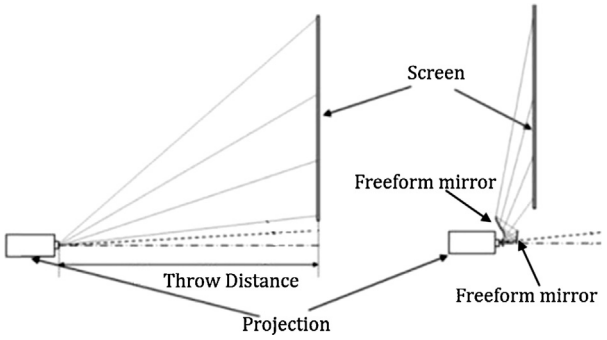

Fig. 10. External freeform optics (right) allows a conventional projector (left) to be nearer to the screen [12].

Fig. 10 shows a new compact video projection optics system with a short throw distance and a wide projection angle using freeform mirrors [12,162]. Freeform prisms can fold the optical path, making the optics smaller, thinner and lighter than with conventional coaxial optics. Olympus Corporation firstly applied a freeform prism to head-mounted display (HMD) in 1998 [86]. Cheng et al. used two freeform prisms to design an optical see-through HMD (Fig. 11), which has a wide field of view of 53.5° and low f-number of (f/#) 1.875 while maintaining a compact, lightweight, and non-intrusive form factor [32]. Two freeform prisms can also reduce the size of the camera module for cellular

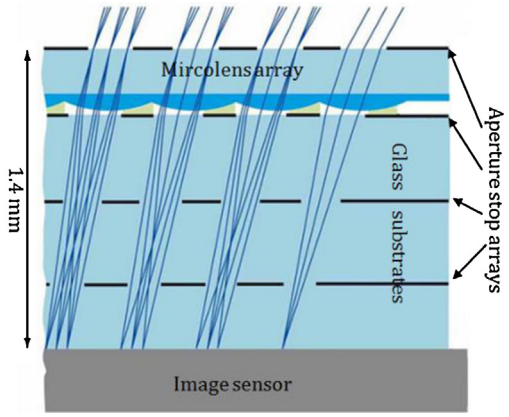

Fig. 7. Ultrathin imaging system using the compound eye based on the planar substrate [25].

Fig. 8. Freeform mirror (above) for panoramic image (below) [82].

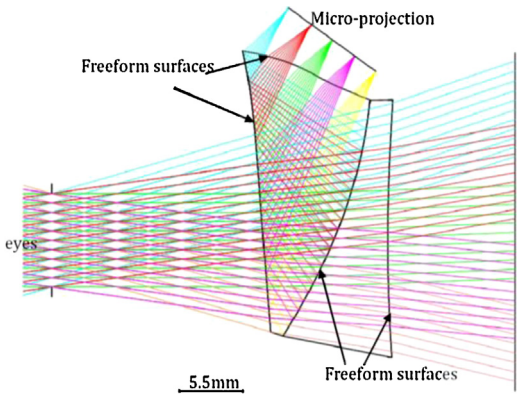

Fig. 11. Optical simulation of FFS prism [32].

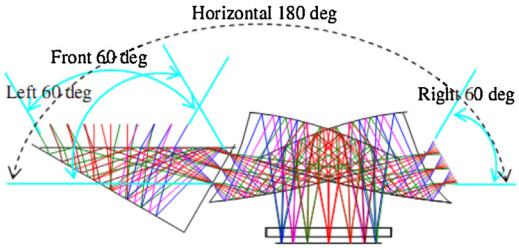

Fig. 12. Optical layout of panorama imaging system using multi freeform prism [214].

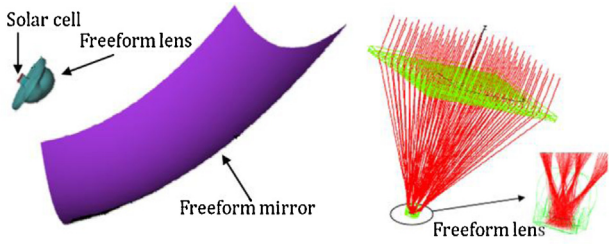

Fig. 14. Off-axis (left) and Fresnel (right) concentrators [256].

phones [214]. Ultrawide-angle compact imaging systems can also be designed by multi freeform prisms (Fig. 12), with good optical performance, 180° field of view of for panoramic imaging [214]. The Ohio State University in USA designed a freeform optical prism array for 3D stereo imaging capability for microscope and machine vision applications [128].

2.2. Concentration application

Non-imaging optics has been pioneered for solar energy concentration, where the goal is to collect the incident light from the large incident aperture in a small exit aperture, driving freeform optics design and manufacturing. Unlike conventional optics, non-imaging optics is concerned not with image quality, but with energy efficiency and distribution. Imaging optics delivers the location and intensity information, while the non-imaging optical system redistributes the energy [242].

The first concentrator for solar energy concentration, the compound parabolic concentrator (CPC), accepted large angle incident light and required no tracking for a small acceptance angle [72,242]. LPI designed a variety of concentrators based on the simultaneous multiple surface (SMS) method. In 1992, the RR (refractive–refractive) concentrator was published, giving large acceptance angle [153]. Next the XR (reflective–refractive) concentrator (Fig. 13) achieved a high efficiency with a low aspect ratio (thickness to entry aperture diameter ratio) and high concentration; the uniformity of the radiation on the cells can be improved by using a Kohler integrator [1]. RX (refractive–reflective) solves the encapsulation problems of XR [148]. The RXI (refractive–reflective–total internal reflection) has also two optical surfaces, but unlike the RX, the rays are directed to the receiver. The main advantage of the RXI concentrators is that the active side of the receiver which is facing the concentrator's aperture makes the bottom of the battery package easier. Because of using a total internal reflection (TIR), the concentrator can be smaller and obtain a higher concentration. By injection moulding, RXI concentrator can greatly reduce costs, but it still has the problem of shadow [154]. In order to solve the shadowing problem and maintain the characteristics of high optical efficiency, simplicity and compactness, TIR–R was designed, which included two parts, i.e., the primary surface TIR surface as a microstructure with infinitesimal flat facets and the secondary refractive surface. The aim of this design is to avoid the metalized surfaces that cause reflection losses and are difficult to manufacture, and to optimize the position of the receiver element's placement for encapsulation, heat sink and electrical connection. A 1256× concentration device has a theoretical efficiency of 100% (without optical losses) with an aspect ratio of 0.34 [1,177].

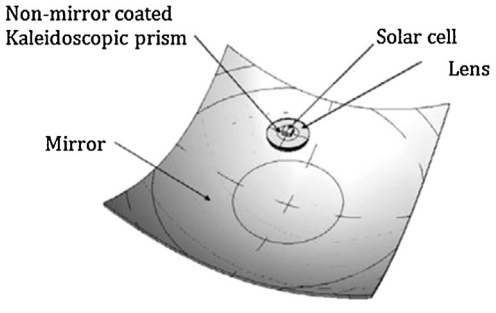

Fig. 13. Perspective view of XR concentrator [1].

A high acceptance angle is key feature for the photovoltaic concentration. Freeform mirrors or lens were applied to Fresnel and off-axis concentrators to improve the acceptance angle and the overall efficiency (solar to electric energy), as shown in Fig. 14 [256]. Freeform optics in non-tracking solar concentrator systems give greater economic benefits.

2.3. Illumination application

Design of high efficiency non-imaging optical systems requires a different approach from conventional imaging optics. The recent emergence of LEDs as a high brightness source has complicated the issue because of the variation of source characteristics in different LED designs [158]. For illumination applications, in particular, it is important to control the intensity distribution. Freeform optics provide uniform, high quality lighting for LEDs application due to its ability of controlling lights exactly.

Design of the optical system to use LEDs as high-brightness sources of projectors is more challenging than when using compact arc lamps. Fournier and Rolland [66] described a system was designed to obtain high brightness LED projection displays. The light engine efficiency was increased by using freeform components adapted to the shapes and the emission patterns of the LEDs considered. Freeform optics has also been used to enhance the angular colour uniformity (ACU) of a white LED and obtain a large angular range of uniform illumination [230]. LEDs are also used in the road lighting systems. A freeform lens was optimized to produce a controlled luminance distribution on the road surface and improve the overall road surface luminance uniformity [62]. The light engine fulfils coupling the light emitted by the source to the microdisplay and projection optics efficiently. A single-element compact freeform lightpipe was designed by non-imaging optical design methods to collect and integrate light in LED projector light engines. Simultaneous optimization of the output surface and the profile shape yields transmission efficiency within the étendue limit up to 90% and spatial uniformity higher than 95% [67].

A freeform microlens array was designed for use with LEDs based on Snell's law and the edge-ray principle. A secondary optic redistributes any illumination profile onto the target surface to achieve prescribed uniform illumination. Depending on the practical illumination requirements, the surface shape of the single freeform microlens can be calculated by the ray tracing method and B-spline fitting. Fig. 15 shows schematic ray path and structure of the micro-lens freeform optics design for LED illumination [210].

Fig. 16 shows a freeform device (called RXI) with Kohler integration for automotive applications, proved to perfectly control bundle of rays issuing from the LED chip corners. This strategy allows the obtaining of intensity patterns quite insensitive to the source (LED) positioning errors [152].

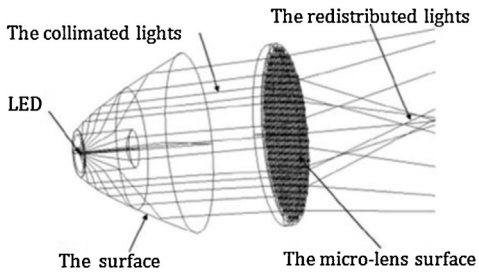

Fig. 15. Freeform microlens for LED illumination [210].

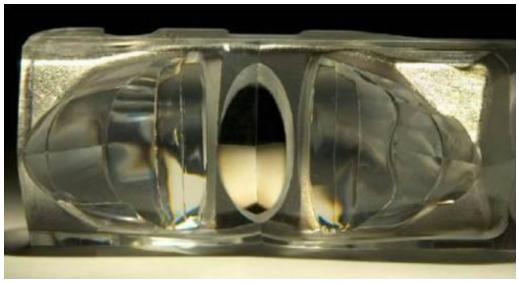

Fig. 16. Freeform Kohler integrator RXI for illumination [152].

Source mask optimization (SMO) has been identified by industry leaders as the only practical method to reach the 22 nm node of optical lithography [122]. To fully realize the potential of SMO, next-generation source definition optics must create exceedingly precise freeform pupils. Diffractive optical elements (DOEs) are integrated in the illumination systems of process control equipment to shape and control the beam for high accuracy inspection requirements [208]. Special illumination patterns, such as annular, dipole, quasar, and so on are commonly used in optical lithography. Wu et al. show a freeform lens array for optical lithography that increases the energy efficiency and reduces the complexity of the exposure system [243]. Fig. 17 shows the optical system and one of the patterns obtained using this freeform optics.

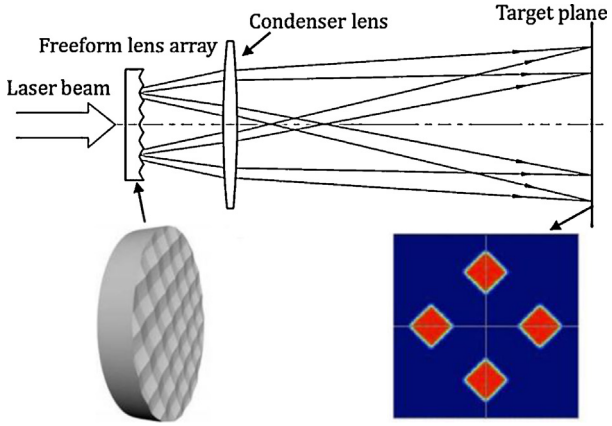

Fig. 17. Freeform lens array (left) in optical lithography and the projection pattern (right) [243].

2.4. Others applications

Freeform optics is also used in laser beam shaping applications. Oliker designed a two-mirror optical system for reshaping the irradiance distribution for a laser beam [170]. The design equations are derived in a rigorous manner and are applicable to a two-mirror optical system not limited to radiance profiles and beam cross sections that are rotational or rectangular symmetric. Smilie et al. proposed a refractive two freeform surfaces system that converts the Gaussian irradiance of an incident laser beam into a nominally flat-top output spot [206].

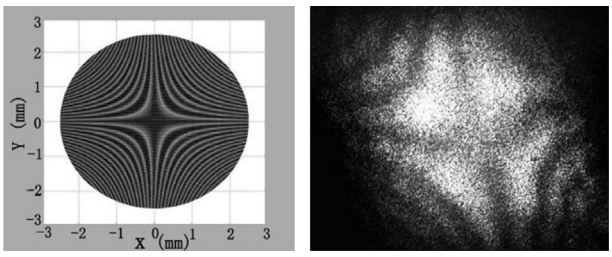

Fig. 18. Laser beam interference patterns by simulation (left) and experiments (right) [232].

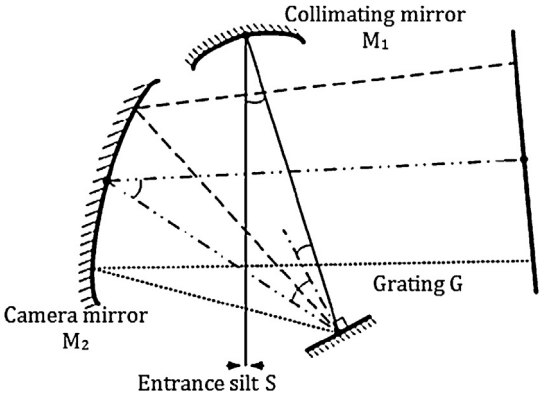

Fig. 19. Optical structure of Czerny-Turner spectrometer [246].

A helicoid mirror with a tilted parabolic generatrix has been applied as an optical delay line. When the mirror rotates, its reflective path varies in the linear and periodic way. The accuracy of optical delay line is better than 6 fs. The mirror is widely used in high-speed optical delay line applications, especially used in the rapid and real-time terahertz time-domain spectrum display system. Fig. 18 shows simulated and measured interference patterns between the reflected laser beam and the incident laser beam. The results agree quite well [231].

Freeform mirrors have been used to solve the problem of astigmatism in traditional Czerny-Turner spectrometers. Ray-tracing result has shown a reduction in sagittal spot size from several hundred micrometres to around 10 μm in the wavelength range from 200 nm to 800 nm. The structure of a typical Czerny–Turner reflective grating spectrometer is shown in Fig. 19, where camera mirror M_2 is a freeform surface [246].

Freeform optics has also been used in a green laser calibration system. Two aspheric-cylindrical surfaces gave appropriate energy concentration of the Gaussian distribution of laser source [33].

3. Mathematics in freeform modelling

Design and machining of freeform surfaces require an accurate mathematical description. The most common ways to describe optical freeform surfaces are:

- Freeform surfaces expressed by specific mathematic formulae. For instance, the double sinusoid surface can be described with sine and cosine functions [257].
- Surfaces described by general XY polynomials, as has been used routinely in commercial optical design software.
- Surfaces described using NURBS, suitable for CAD modelling software. Commercial optical design software also supports this data format [18].

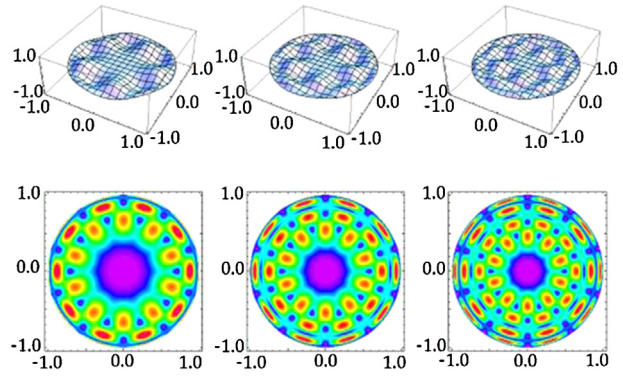

Fig. 20. Plots (above) and modulus of their gradient (below) of the basis function [65].

- Surfaces expressed by truncated functions to describe the step surface, and using the mathematic transformation to describe the array structure.
- Surfaces represented as the linear combination of basis functions, such as Zernike polynomials commonly used in optical design and fabrication.

Aspheric optical surfaces have traditionally been described starting from a conic expression, for example:

$$z = \frac{c(x^2+y^2)}{1+(1\text{-}(1+k)c^2(x^2+y^2))^{1/2}} + \sum_{m=0}^{p}\sum_{n=0}^{p} C_{mn}x^m y^n \quad (1)$$

where c represents the curvature of base surface, k is the conic constant, and C_{mn} are the coefficients of xy terms. This formulation is not based on an orthogonal expansion and the coefficients are not individually physically meaningful. Recently, there has been growing interest in alternative representations based on linear combination of basis functions. Forbes proposed Q-polynomial surfaces, an orthogonal sum of Jacobi polynomials, for axisymmetrical aspheres. The polynomial coefficients can be directly related to slope enabling intuitive evaluation of the fabrication difficulty and assembly sensitivity [64]. Another set of basis functions provide robust and efficient algorithms for characterizing freeform surface as well as computing derivatives to any order [65]. Fig. 20 shows the plots and modulus of their gradient of the basis function of $u^5\cos(5\theta)Q_n^5(u^2)$, where n is the order of polynomial and equals 1–3.

Some basis functions dominate optical testing result, for example, the Zernike polynomials represent the wavefront and all kinds of aberrations [245]. Fig. 21 shows 15 Zernike polynomials, where Z_n is the nth entry in one of the different orderings of Zernike polynomials. Other basic polynomials, such as Gaussians [28], modified Zernike polynomials [247] and Φ-polynomial [29,111], have been proposed to facilitate optimization. Cakmakci et al. [28] indicate that a linear combination of Gaussians enable optimization to a better MTF than XY or Zernike polynomials [28].

4. Optical design

There are two strategies for optical design of freeform optics: multi-parameter optimization and direct mapping [10]. In multi-parameter optimization the optical requirement is defined as a quantitative merit function that is to be minimized by optimization. However, when optimizing freeform optics, the higher order polynomials required for complex surfaces can make optimization slow. The direct mapping method is called source-target mapping, which defines a truly accurate freeform solution that takes the light from the source distribution to the desired target distribution. The surface feature points are obtained using this method, and then modelled by fitting or interpolation to get freeform surfaces. Several important direct mapping methods are introduced below.

4.1. Partial differential equations

This method, in essence, is to establish the relationship between the three normal vectors of incident surface, target surface and freeform surface by solving the partial differential equations as shown in Fig. 22 [187]. The partial differential equation is based on the energy conservation and tailoring theory, which redistributes the radiation of a given small light source onto a given reference surface, achieving a desired irradiance distribution. The tailoring method was introduced in 1993 by Winston et al. A freeform reflector was firstly designed by solving a differential equation coupling the angle of incidence and target surface illumination distribution [198]. The edge-ray principle is a fundamental theory of the tailoring method, verified in 1994 using geometrical optics [188]. Rabl et al. obtained a solution for extended sources (cylindrical sources) by establishing differential equation, instead of the point source [184]. In 1996, Ong defined the method for extended source as tailored edge-ray designs (TED), and gave the governing differential equations, i.e., the analytic solutions but not simple closed-form solutions [171]. In 1996, Jenkins et al. gave much more compact reflector shapes by a new integral design method based on the edge-ray principle. In addition, the reflectivity of the reflector is incorporated as a design parameter [101].

Harald et al. used freeform elements to attain a desired irradiance distribution by using the tailoring method. The freeform lens was formed by solving a set of partial nonlinear differential equations with the curvature and slope. The irradiance distribution shaped as the letters "OEC", which is the abbreviation of "Optics & Energy Concepts", was obtained on the target as shown in Fig. 23 [187].

Harald et al. presented the 3D tailoring method in 2003, which is based on the principles of interaction of light rays with an optical

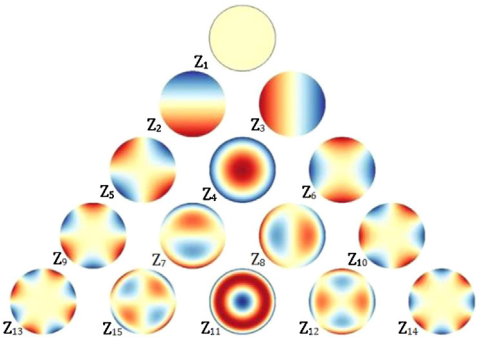

Fig. 21. The first 15 Zernike polynomials.

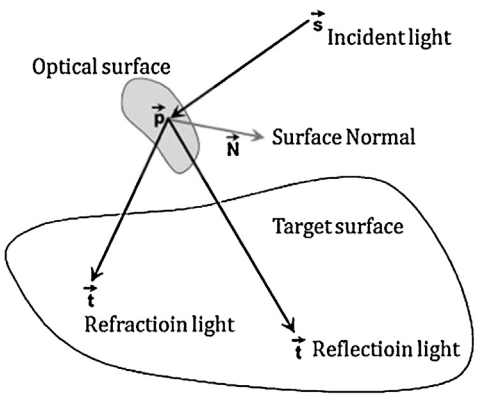

Fig. 22. Principle of partial differential equations [187].

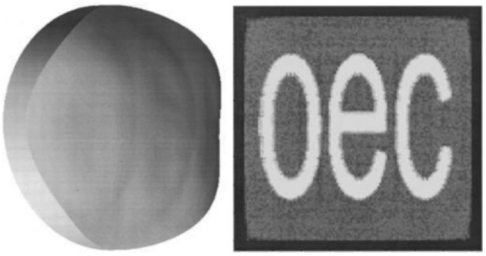

Fig. 23. Freeform lens (left) and irradiance distribution (right) [187].

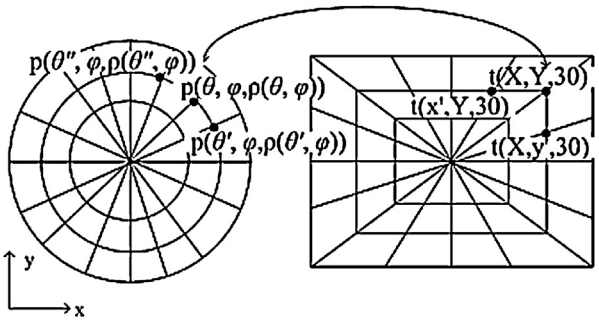

Fig. 24. Principle of point-to-point mapping [176].

surface in combination with differential geometry of the freeform surface. This method obtained a uniform distribution over large lighting areas for use in street lighting, emergency lighting, office lighting, ambient lighting and special lighting [220]. The uniformity of the tailoring method is also important. In 2008, a uniformity study was conducted for LED lighting, and the uniformity up to 90% was obtained [43,79].

If the surface is more complex, the solutions of nonlinear partial differential equations can become more difficult. In recent years, a quite general approach combining geometric techniques with methods from calculus of variations was developed and applied to a rigorous and unified investigation of several classes of such equations. This approach allows implementation of provably convergent numerical algorithms. The trajectory equation at the interface of the light is obtained using Fermat theorem and mathematical derivation. This formula can be used to derive the mapping about the object and image then to get the freeform surface. Oliker has made a comprehensive study in this method [115,168,169]. The approach is based on a rigorous mathematical theory and does not assume rotational or any other symmetry of the data. Therefore, it avoids the complicated process of solving partial differential equations.

The partial differential equations method is generally limited to point sources, although part of an extended light source with limited shapes (such as rectangular or tubular) can also be calculated. The calculation process is very cumbersome. In addition, it is difficult to establish the exact nonlinear partial differential equations, and one can only calculate one freeform surface at a time.

4.2. Point-to-point mapping

This method establishes the equation between the lighting energy emitted by the source and the lighting energy obtained by the target based on the conservation principle. Then the coordinates and normal vector of surface points are obtained by iterative solution to get the surface form. The point-to-point mapping method was proposed by Parkyn [176] for general illumination tasks in 1998. The source and target surfaces are divided into grids, whose relation is defined using extrinsic differential geometry (EDGE) to obtain the normal vectors of the lens to generate a smooth surface. One of the grids has cells which vary in solid angle such that each encompasses the same luminous flux. The other grid having the same topology and number of cells is formed according to the intensity distribution of the source. As shown in Fig. 24, the right grid expresses the prescribed intensity distribution while the left expresses the angular distribution of light emitted by the source.

In 2006, Parkyn applied a new pseudo-rectangular spherical grid to establish correspondence between source-grid cells and the rectangular cells of a target grid. He obtained the central spines by a linear integration, after obtaining the adjacent rows successively in a lawnmower fashion [175].

There are studies to combine this method with other techniques. For example, it was combined with Monte Carlo ray tracing to complete the LED package for high-performance LED lighting in 2010 [229]. A gradient method with optimization calculation was proposed to get accurate curved surfaces from a point source. The method represents the surface of an element in terms of the distribution of the eikonal of light field in an adjacent plane based on gradient minimization of an error function that represents the difference of the calculated and specified irradiances in 2008 [9]. In 2010, a feedback modification method was proposed to design freeform optics with uniform luminance for LED sources based on variable separation mapping. In this method, the non-negligible size of a LED source is taken into account, and a smooth freeform lens with rectangular luminance distribution designed. The luminance uniformity is improved from 18.75% to 81.08% after eight times feedback [136].

4.3. Simultaneous multiple surface (SMS) method

SMS method, an important breakthrough in freeform optics, was invented in 1990 for the 2D non-imaging optical design. The abbreviation of SMS comes from the fact that it enables the simultaneous design of multiple optical surfaces. The original idea came from Minano, and the first implementation to 3D geometry came from Benitez. Therefore, SMS also is called the Minano–Benitez design method [242].

The principle of SMS is "bundle-coupling" and "prescribed-irradiance". "Bundle-coupling" means that input and output bundles are coupled, that is to say, any incident rays entering into optical system would go out the exit pupil. "Prescribed-irradiance" means one bundle must be included in the other, that is to say, SMS couples two input wavefronts into two output wavefronts. Freeform surfaces calculated by SMS have the features of compactness, efficiency and simplicity [11]. Fig. 25 shows one case of 3D SMS, which provides an image-forming design whereby the light source is placed on the object plane and the target on the image plane. In Fig. 25, points A–D are object points while A′–D′ are their corresponding image points. Two freeform mirrors, the primary optical element (POE) and a secondary optical element (SOE), can be calculated using the SMS method.

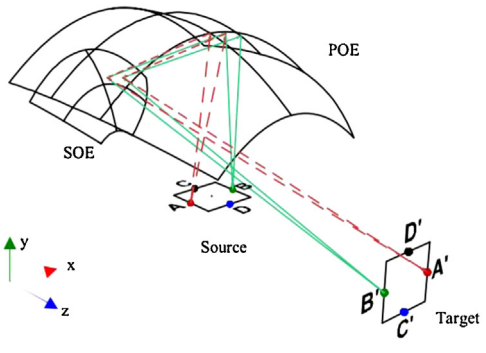

Fig. 25. The principle of 3D SMS [152].

SMS has many advantages compared with other methods. For instance, SMS is based on the edge principle and Fermat's theorem. SMS can be used in designs for point and extended light sources. A freeform condensor, for example, was designed to obtain the rectangular entrance for arc lamps or halogen bulbs [151]. SMS can be used to take the size and angle of the source into calculations. The 3D SMS is at present the most powerful direct design method for illumination devices using extended sources [152]. SMS can be used to design at least two free surfaces in one time. For the concentrator, the traditional free-form surface design method limits the distribution of illumination and maximum concentration and requires a linear or a spherical surface, but the SMS does not have these requirements. SMS can be used in both imaging and non-imaging optics. Fig. 10 is one imaging example designed by SMS method for the projection with short throw distance.

5. Machining mechanism

Freeform optics can be machined by a variety of methods, including ultra-precision cutting, grinding and polishing. The earliest method used in finishing of optics was polishing. Grinding has been used for centuries for machining optical blanks, but grinding with nanometric precision has not become available before the advent of ultra-precision machines. Grinding is well suited to hard and brittle materials, such as glass, silicon and steel [21] but can have low efficiency, and high cost, and limitations for complex surfaces. Single-point diamond cutting can fabricate optics without the subsequent finishing for some materials.

In order to get the nanometric surface finish, or realize the cutting of brittle materials, the ductile-mode material removal is important for ultra-precision cutting or grinding. In nano cutting, undeformed chip thickness has been reduced to nanometric scale. In this scale, due to the tool edge radius and the size effect, the mechanism of material removal is different from the conventional shearing model proposed by Mallock in 1881 [139] and Merchant in 1944 [147]. The significant tool edge radius compared to the undeformed chip thickness causes the negative effective rake angle, which produces the necessary hydrostatic pressure enabling ductile deformation in front of the tool edge, avoiding the fracture of brittle material [61]. Schinker et al. showed that hydrostatic pressure with overlaid shear stresses is a prerequisite for ductile machining of glasses [196,197]. This condition can be met by applying cutting tools with negative effective rake angle for cutting processes and bonded abrasives for abrasive processes. Due to this machining mechanism, brittle materials can be machined with "ductile-mode" material removal [21,58,61].

The material removal mechanism of optical glass by grinding strongly depends on the undeformed chip thickness. With increasing undeformed chip thickness until a critical value, high hydrostatic pressure is maintained, which is the prerequisites for crack free and ductile grinding. The contact of the abrasives with the machined substrate leads to elastic material response and plastic behaviour [21]. These mechanism and results have been demonstrated in single grain cutting experiments of glasses [157,197] and technical ceramics [213,221].

The nano cutting mechanism of monocrystalline silicon was investigated using molecular dynamics (MD) or finite element (FE) analysis [116,251]. A model of chip formation in nano cutting was based on extrusion, rather than earlier explanations using shearing, and was verified by the taper cutting experiments [57,58,61]. It is generally considered that there is a phase transition from Si-I (diamond cubic) to Si-II (metallic state) under loading [249]. The amorphization process can be produced in material removal due to the hydrostatic pressure. Therefore the material around diamond tool becomes ductile enough to be extruded and form the continuous chips. On unloading, the phase of silicon transforms from Si-II to amorphous silicon. Although brittle materials could be machined in ductile mode when the undeformed chip thickness reduced to nano-scale, the poor processing efficiency and short tool life still prohibit the single point diamond machining from fabricating the optical crystal widely. Nanometric machining of ion implanted materials (NiIM) was proposed by modifying the mechanical properties of the surface layer to be machined [55]. The implanted F ions soften the surface layer of single crystal silicon and make the ductile–brittle transition depth much deeper. Optical freeform surfaces have been successfully machined to prove the practicability of the NiIM approach, and the surface roughness of 0.86 nm in Ra was achieved.

This amorphous modification can be demonstrated using appropriate characterization methods. Amorphous silicon can be detected by Raman spectroscopy [76], TEM [58] and so on. Fig. 26 shows the TEM analysis of the cutting chips reveals that single crystal silicon undergoes phase transition during machining [57]. The existence of amorphous state indirectly verifies the transition from Si-I to Si-II. Some other experiments can prove the silicon's phase transition directly, such as detecting the electrical property changes during nano-indentation [17]. The decrease in the resistance during loading was induced by the formation of Si-II phase, and the increase during unloading proves the phase transforms from Si-II to amorphous silicon, as shown in Fig. 27.

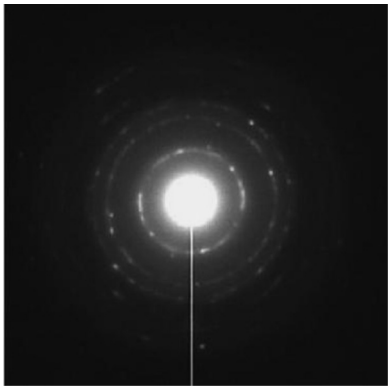

Fig. 26. Typical electron diffraction pattern for the silicon chips showing the presence of polycrystals [57].

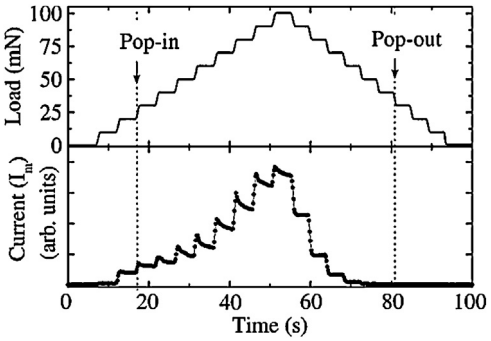

Fig. 27. Applied load and current as a function of time during indentation loading in crystalline Si [17].

6. Machining approaches

Recently, the slow slide servo and fast tool servo emerge for diamond turning. They get rid of the limit of machining freeform surfaces, making the ultra-precision cutting recognized as the most effective method [30,40,219]. Grinding, milling and other methods are also developing to be suitable for the fabrication of some kinds of freeform optics or materials.

6.1. Slow slide servo

Slow slide servo (SSS) or slow tool servo (STS) is an approach to upgrade a standard two-axis diamond turning machine, while a high-precision *C*-axis encoder is mounted to the spindle. Therefore, SSS is actually a type of turning method with *C*-axis controls and T-shape configuration, in which the *Z*-axis oscillates back and forth while *X* and *C* maintain constant speed [26,222]. A cylindrical machining method was presented using the *XZC* axis in the cylindrical coordinate system, with the cutting path for freeform optics also designed in cylindrical coordinate [60].

SSS is slow because the *Z*-axis, on which the tool is mounted, is massive and the motor that drives it can only produce limited speed and acceleration. Compared to fast tool servo and diamond milling, SSS has the longest machining time. However, SSS gives better surface finish and can give azimuthal height variations of more than 25 mm, which is a major advantage [40] for certain freeform optics.

Synchronous multi-axes motion control is a key to all freeform optics machining processes. In current implementations of SSS typically the spindle is controlled using the precision direct current motor, and *X* and *Z*-axes are controlled by the linear motor.

Many workers have considered machining trajectory, compensation of diamond tool and system error analysis. In the precision path design method [60,257] the tool parameters, including tool nose radius and clearance angle, are considered in compensation. The tool parameters are selected to avoid cutting interference considering the tool nose radius, included angle, clearance and rake angles. The form accuracy in aluminium alloy materials using the designed path can be 0.5 μm PV. Fig. 28 shows typical freeform surfaces produced using the cylindrical coordinate machining. Yi et al. fabricated phase plates using SSS to compensate the wavefront aberrations of human eyes. The maximum shape error obtained was 0.8 μm. The influence of the position of the phase-plate relative to the pupil has been considered and the practical utility of this mode of aberration correction was investigated with visual acuity testing [253].

Fig. 28. Typical freeform optics fabricated by the cylindrical machining method [61].

Slow slide servo machining is an efficient method to fabricate the off-axis aspheric mirrors on axis. Dai et al. predicted 3D topography of SSS machining for the off-axis aspheric form [37,255]. However, it is still difficult to machine off-axis aspheric mirrors with a large ratio of sag height to diameter because of tool interference. One method, coordinate transformation machining, can be used to make the machining feasible by reducing the ratio of sag height to diameter. Freeform prisms were experimentally machined to demonstrate that the method also works well for complex surfaces [258].

SSS is an important method to fabricate the structured optics, such as aspheric lens arrays. A 5 × 5 microlens array was fabricated on 715 nickel alloy and 6061 aluminium alloy [254]. Huang et al.

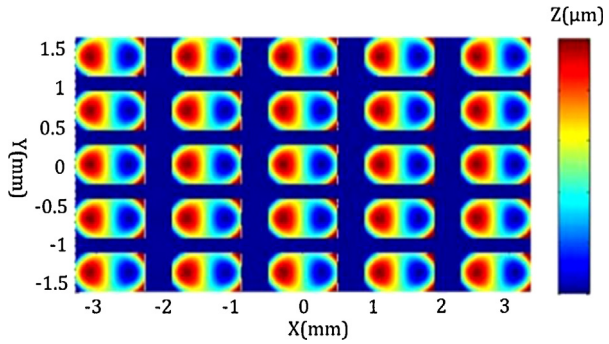

Fig. 29. Alvarez lens array model [90].

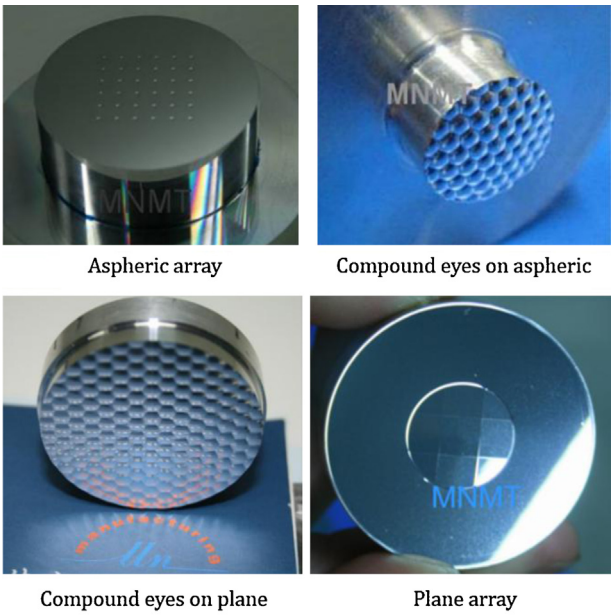

Fig. 30. Compounded eye and other structured optics fabricated by SSS method.

also fabricated a micro Alvarez lens array, consisting of a pair of identical bi-cubic phase profile optical lenses (Fig. 29). An Alvarez lens can be used for dynamic correction of arbitrary astigmatic aberrations by relative translation of the bi-cubic [88]. Zhang et al. implemented SSS to fabricate the structured optics based on curved substrate, such as compound eye, as shown in Fig. 30. To avoid the shape distortion caused by tool misalignment, an off-centre machining configuration was used to improve the form accuracy [259].

A similar configuration to SSS was studied, in which the *XCB* axes synchronously move. A machine equipped with an additional rotational axis can create motion in the *Z*-direction by rotating the *B*-axis with a tool mounted off centre as shown in Fig. 31. For steep

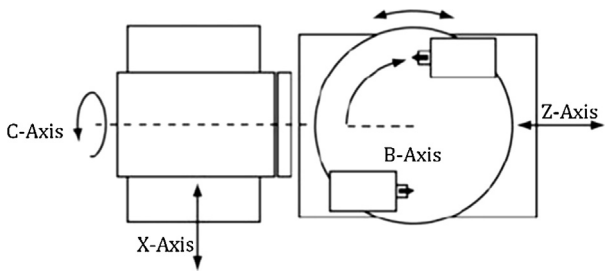

Fig. 31. XBC STS configuration [41].

surface slopes, a mild freeform shape would require large motions of *Z* axis, but only small motions of *B* axis. The reaction forces from *B* accelerations excite the machine base in the less sensitive angular direction, and the ratio of moving mass to reaction mass is much lower for *B* acceleration than *Z*. XBC SSS machining is feasible but it is still in the early stages of development relative to the more mature *XZC* configuration [41].

Conventional SSS is limited in its ability to fabricate multi freeform surfaces on one lens, such as the freeform prism, as shown in Fig. 11, which needs positioning accuracy between different freeform surfaces. A machining method combined SSS method and fly-cutting method was used to machine this type of lens maintaining the accuracy of relative positions [260].

6.2. Fast tool servo

A linear actuator driving an ultra precision lathe and its driving controller, called as a fast tool servo system, was described by Patterson et al. in 1985 [178]. Fast Tool Servos (FTS) still employ T-type configuration similar to *XZC* SSS machining. The FTS generates the high frequency movement in the *Z*-axis by a specialized control system of a short travel system superimposed on the original axis-control of the machine. The FTS generates accurate *Z* axis feed based on the desired surface and the machine axes positions. FTS is commonly used to diamond turn surface structures such as micro prisms, lens arrays, torics and off-axis aspherics with small sags (up to hundreds of microns) [19,172].

FTS can be classified by their drive mechanisms into PZT actuators driving voice-coil motor (VCM), Maxwell electromagnetic force (MEF), servo motors, magnetostrictive actuators and so on. The first three methods are more commonly used. Most papers report the applications that improve machining accuracy of FTS, decrease fabrication error, and process non-circular surfaces. Most FTS are driven by PZT actuators, with the advantages of fast response, simple driving principle, and high stiffness; these systems have strokes from several to a few hundred micrometres with frequencies from 20 Hz to 2 kHz. Flexures or stacks can amplify the stroke of FTS driven by PZT. FTS driven by VCM can travel several millimetres with good dynamic characteristics and linearity. However, FTS driven by VCM have lower frequency response and lower accuracy compared with FTS driven by PZT.

MEF–FTS can realize short (below 100 μm) and medium (100 μm^{-1} mm) strokes, and adopts a biased permanent magnet method for linearity. Such FTS have good dynamics and large acceleration, allowing very high frequency response. Gutierrez et al. designed an MEF–FTS with a stroke larger than 800 μm and the band width of 200 Hz [77]. Trumper et al. built an MEF–FTS with the stroke of 30 μm and the bandwidth of 23 kHz [135,225].

Brinksmeier et al. designed two nano-FTSs (nFTS), featuring strokes of 500 nm and 350 nm at frequencies up to 5 kHz and 10 kHz, respectively [22]. Using a special piezo ceramic, this has high linearity, near zero hysteresis, and negligible heat dissipation properties which enable an open-loop control of the system. The designed nFTS can generate a variation of the undeformed chip thickness within nanometer range enabling the processing of diffractive micro-structures. Morimoto et al. designed a new FTS drive using hydraulic amplification giving a system frequency response of 50 Hz with a stroke of 100 μm, which is 4 times larger than the basic design [159]. Gao et al. also designed an FTS system using a PZT to actuate the diamond tool and a capacitance probe for feedback, (Fig. 32), giving a bandwidth of approximately 2.5 kHz and a tool displacement accuracy of several nanometers in the closed-loop mode. This system was implemented to fabricate the sinusoidal waves in the *X*-direction and the *Y*-direction with spatial wavelengths of 100 μm and amplitudes of 100 nm over an area of 150 mm [71]. The newly designed FTS can fabricate difficult-to-cut materials such as steel, brittle materials, and so on. Mizutani et al. employed an FTS with resolution of 5 nm in grinding machine to generate a ceramic mirror-surface with the accuracy of ±0.01 μm

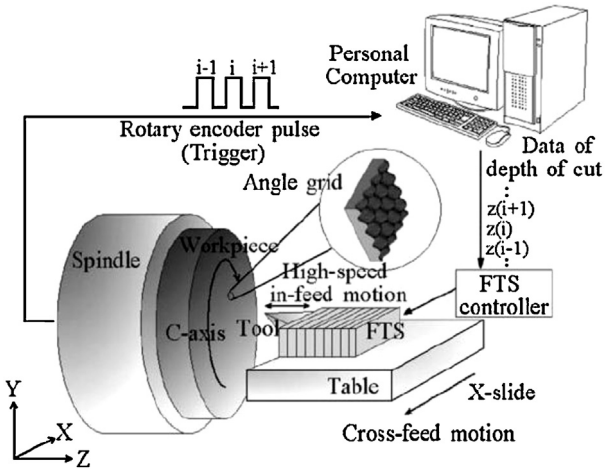

Fig. 32. FTS machining structure for sinusoidal waves [71].

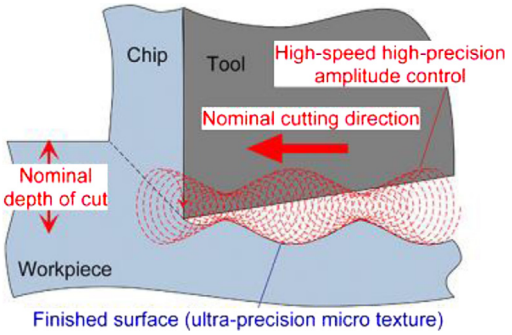

Fig. 33. Elliptical vibration FTS [212].

[156]. Suzuki et al. designed an FTS whose depth of cut can be actively controlled in elliptical vibration cutting by controlling vibration amplitude in the thrust force direction as shown in Fig. 33 [212].

FTS with high frequency response always have short strokes, and FTS with large strokes always have low frequency response and relatively low accuracy. Therefore many researchers put their efforts on hybrid FTS in order to realize an FTS with both high frequency response and large strokes. Elfizy et al. [49] designed a dual-stage FTS features with large range of linear motor and high frequency response and high accuracy of PA. They utilized flexures to provide precise frictionless motion. The dual-stage FTS have the maximum stroke of 1 mm, resolution of 20 nm, frequency response of 50 Hz with small amplitude motion, natural resonant frequency of 650 Hz, and can be applied to process sinusoid curve in ultra-precision milling machine [49]. FTS combining the VCM as macro stage and PA as micro stage is also widely adopted by researchers like Liu et al. who obtained the maximum stroke of 1 mm and a frequency response of 200 Hz [132]. Liu et al. applied a FTS combining linear motor and PA in ultra precision milling machine. The FTS can realize the stroke of 20 mm with positioning accuracy of 0.2 μm and tracking accuracy of 2 μm, it can be applied in ultra-precision machining [133]. Li et al. developed a FTS combining a stepper motor for the coarse motion to obtain the large stroke and fast response speed, and a piezoelectric micro-actuator for the fine motion to achieve high resolution and accuracy. The experimental results show that the stepper motor has a working stroke of 90 mm with the displacement resolution of 0.3 μm and the piezoelectric micro-actuator has a working stroke of 40 μm with the positioning accuracy of 0.9 μm [126].

Tool path is also important for FTS machining to control the shape accuracy and surface quality. Scheiding et al. discussed the Cubic Spline interpolation and tool radius correction of cutting tool path to fabricate the micro optical lens array on a steep curved substrate [194].

6.3. Ultra-precision milling and fly-cutting

Ultra-precision milling is suitable for the fabrication of micro-structured optics, which are widely applied in both imaging and lighting. One configuration, called a broaching process, use a multi-axes machine for cutting the surface, with a straight line tool path in projection. Fig. 34 shows a unique freeform microlens array for a compact compound-eye camera that gives a large field of view of 48° × 48° with a thickness of only 1.6 mm [129,130].

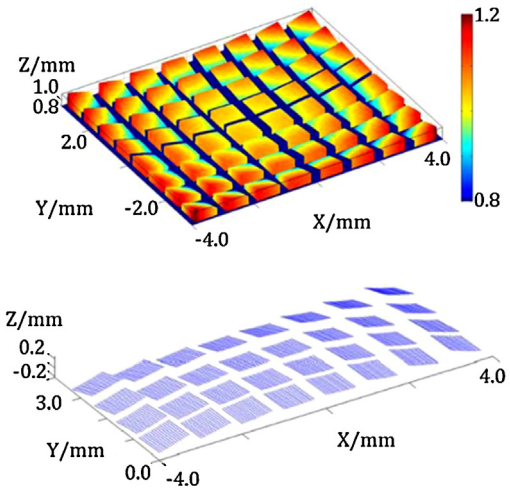

Fig. 34. Freeform microlens model (above) fabricated by straight line cutting path (below) of broaching process [129].

Ultra-precision milling always uses a high-speed spindle for high performance. The easy approach is that the diamond tool is mounted onto the spindle of an ultra-precision turning machine and the part where the tool post is normally situated; this method is called fly-cutting. It only needs the *X* and *Z* two-axes motion, and the tool feed direction is perpendicular to the spindle rotational axis for nominally plano surfaces; More complex surface shapes can be produced, particularly on machines with a *B* axis. Fly-cutting is commonly used to fabricate the micro-grooves, so that it is also known as diamond grooving. As with textured cylindrical roll turning, burrs are a major problem. An experimental set-up for machine micro-grooving was presented and the burr formation mechanism have been discussed both theoretically and experimentally [56,59]. A small uncut chip thickness helps reducing the burr formation. Micro grooves machined by down-cut method using a cutting tool with "perfect" edge profile geometry resulted in a burr-free groove with accurate profile.

A microprism array is a pyramid array which can be formed using the three-step micro-grooving by fly-cutting. Such structures are commonly used to passive lighting applications, especially in traffic signals (Fig. 35(c)). Fig. 35 also displays the other micro-structured surfaces machined by fly-cutting [56].

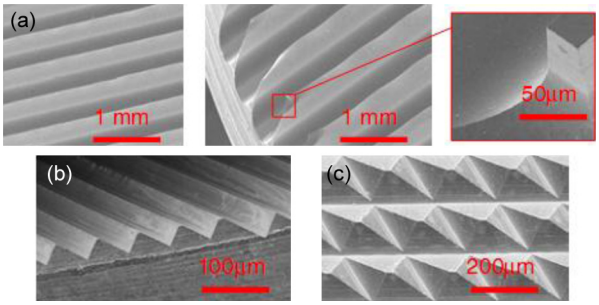

Fig. 35. Typical micro-structured surfaces fabricated by fly-cutting [56].

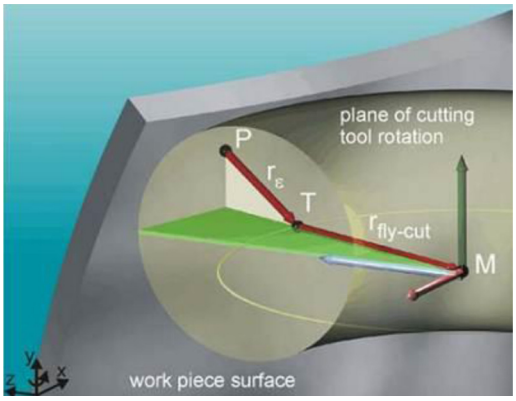

Fig. 36. Tool path generation of raster milling [24].

As indicated above, a rotating diamond tool can also be mounted on the multi-axes machine. The machining configuration is similar to fly-cutting, although if the diamond is close to the axis of rotation, this process is commonly referred to as milling. Often three axes of linear motion traverse either the spindle or the part to contour the freeform shape. The tool always moves in a raster path, so it is called raster milling. Raster milling is a comparatively less efficient process, particularly for long cycle times and susceptibility to external disturbances such as environmental temperature fluctuations. Raster milling is useful for continuous surfaces where tool clearance angle requirements is difficult to be met for other machining methods. The F-theta and hyperbolic parabolic surfaces were fabricated in [24] and [117] using raster milling. The ball-end milling tool was also used in this method, and the cutting strategies, tool path generation, and kinematic errors are analyzed as shown in Fig. 36 [24].

Takeuchi et al. presented a cutting method using non-rotational cutting tool to deal with the manufacture of multiple-focus micro Fresnel lenses [160,216]. The machining is conducted on a 5-axis control ultra-precision machining (Fig. 37). The cutting tool is mounted to the ultra-precision machining centre so that the tool axis can be kept perpendicular to B table and that the top of tool can correspond to the rotational centre of the C table. This method was also used on 6-axis machine to fabricate flat-end curved microgrooves [217].

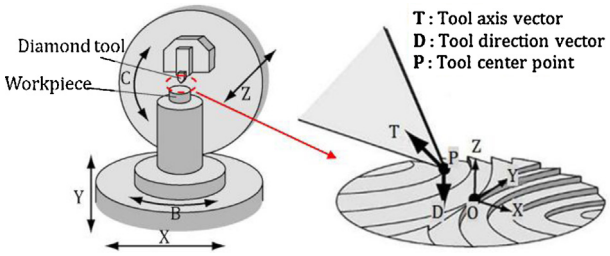

Fig. 37. Non-rotational cutting tool machining [160].

Another approach uses an ultraprecision lathe where an additional high-speed milling spindle is integrated, which holds the diamond tool. The three machine axes are used to position the tool relative to the substrate and to feed the tool on its spiral tool path. When the tool feed direction is normal to the part surface, this method is called end-milling and is suitable for structuring small optics especially ones with high slopes. It is also called micro milling for the tool is smaller than the size of structure. Scheiding et al. fabricated an array containing more than 1300 lenses. The lenses have a design radius of 1.286 mm and a sag of 257 μm [193].

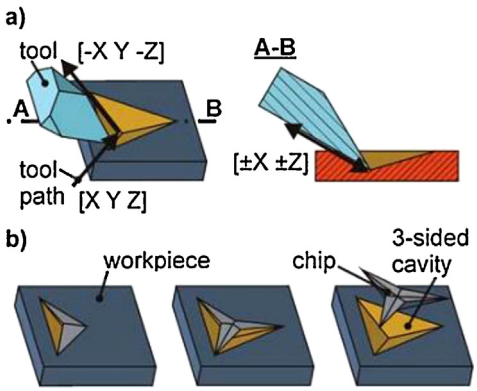

Fig. 38. DMC machining principle [63].

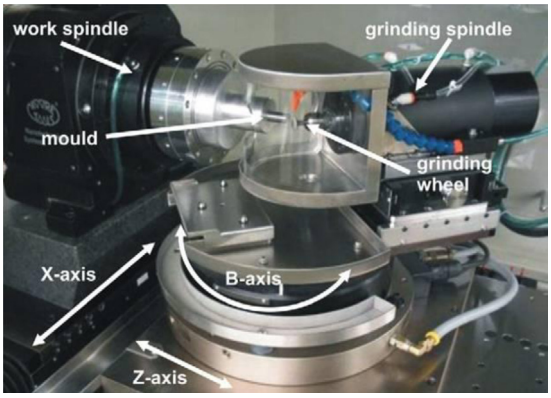

Fig. 39. Wheel normal grinding [21].

End-milling was also applied to fabricate micro-groove and micro-pyramid arrays. Because the tool feed direction is parallel to the end-mill rotational axis, the finished surface is generated by the same point on the cutting edge. Even if the cutting edge is worn, a smooth surface may be obtained. Micro-dimple arrays, micro-grooves, and micro-pyramid arrays with extremely smooth surface and high-accuracy profile could be obtained on oxygen-free copper without remarkable tool wear [250].

Another machining process, diamond micro chiselling (DMC), has been developed. It is capable of generating micro cube corner retro-reflectors with hexagonal individual apertures and 100% of effective aperture. The cutting principle for a three sided cavity is illustrated in Fig. 38. In combined movements of axes *X*, *Y*, *Z* the tool enters the workpiece and a sloped mirror edge is cut. An array of 2500 cubic hexagon retro-reflectors of 200 μm structure size has been fabricated [20,63].

6.4. Ultra-precision grinding/polishing

Diamond machining is well suited to cutting crystal materials such as germanium, zinc sulfide and zinc selenide, as well as polymers such as polymethylmethacrylate, polystyrene, and polycarbonate. Mould inserts, for moulded optics, are manufactured by harder and more brittle materials that cause rapid diamond wear. In addition, the demand for micro glass aspheric and freeform optics is increasing rapidly. Glass has better mechanical and optical properties than plastic for most optical applications. The fabrication of moulds and glass optics needs ultra-precision grinding or polishing. The machining of ultra-high precision parts by abrasive processes, however, can be more difficult than turning and milling due to process complexity and non-deterministic nature [21,205].

In case of freeform optics the machines often have multiple axes with controlled motions; some machines have up to six axes that can be commanded simultaneously. High speed grinding spindles that can reach speed of 200,000 rpm are used to the grinding of brittle materials. In recent years many efforts have been conducted by researchers to determine the best way to grind these mould cavities. Yamamoto [248], Suzuki [211] and Chen [31] describe some of the techniques used in grinding micro mould cavities.

Tohme reported a wheel normal grinding process with two linear axes and a rotary axis. In this case, the working surface of cylindrical or cup grinding wheel is kept normal to the workpiece surface by the control of rotary axis. Therefore, the included angle between grinding spindle axis and surface tangent needs to be kept constant over the entire grinding process, as shown in Fig. 39, which ensures that the tool geometry errors does not affect the shape errors of part. This requires the grinding wheel to be aligned with the *B*-axis centre line [21,223].

Another grinding method has been developed for precision machining of freeform shapes, i.e., freeform wheel normal grinding, which is also called slow-tool grinding. In this method, the workpiece spindle is equipped with a rotary encoder (*C*-axis), so that the position of the grinding wheel can be moved back and forth as a function of the angular position of the workpiece (tool servo). Using this grinding technique, a large number of different lenses and moulds with cylindrical or toric shapes as well as lens arrays can be ground [21,223].

A number of micro grinding processes have been developed in the past years, especially for decreasing the grinding wheel dimensions and increasing the achievable aspect ratio. For the manufacturing of microstructures two notch grinding methods with different tool shapes have been developed [21,23].

Deteministic grinding is difficult mainly due to abrasive grit wear which changes both grinding forces and material removal mechanism. Metrology is always used to compensate the shape error. Electrolytic in-process dressing (ELID) is a good approach in reducing the effect of wheel wear. A half-sphere wheel was designed for freeform optics grinding in ELID, as shown in Fig. 40. This method is named FREEDOM (free dominant machining), which can yield very good surface finish (Sa < 2 nm) and reduced sub-surface damage [166].

Generally, grinding alone cannot meet the optical surface requirements for a wide variety of freeform optics. Hence a subsequent smoothing step is required. Several polishing technologies have been proposed for cost-effective manufacturing of freeform optics, including Magnetorheological Finishing (MRF) and Magnetorheological (MR) Jet, which can produce complex optical surfaces with accuracies better than 30 nm PV value and surface micro-roughness less than 1 nm in rms. MR Jet, a newly developed magnetically assisted finishing method, addresses the challenge of finishing the inside of steep concave domes (Fig. 41) and other irregular shapes [205]. Zeeko has developed a freeform automated polishing process, named as Precessions process, which involves a sub-diameter inflated bulged membrane tool, operating in the presence of polishing slurry [228]. Fig. 42 shows the fabrication of torus surface on glass using this process. Lithography

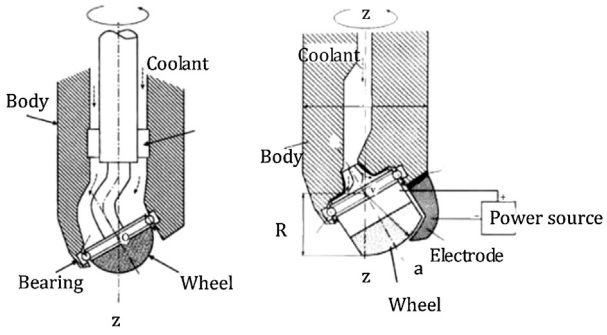

Fig. 40. Half-sphere wheel of FREEDOM using ELID [166].

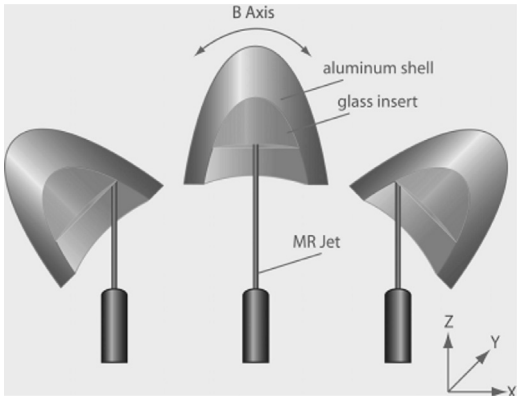

Fig. 41. Concave domes fabricated by MR Jet [205].

Fig. 42. Torus fabricated by Precession process [228].

optics need figure accuracy better than 250 pm rms, especially for the extreme ultraviolet (EUV) lithography. Ion Beam Figuring (IBF), performed by directing a broad beam high current ion source (Kaufman type) onto an optic in a carefully controlled manner, removing substrate material by ion beam sputtering, is suitable for this requirement of lithography optics [227].

7. Moulding technologies

Many small aspheric lenses, such as camera lenses, are made by the direct moulding of glass or plastic in an aspheric mould. The moulds have the opposite shape of the finished asphere and are made from materials that can withstand the required high temperatures [8]. These optical components are readily mass produced by the millions with astonishingly good quality. High quality plastic optics is mass produced by injection moulding [149]. Liquid plastic is forced into a heated mould cavity at high pressures. The plastic is solidified to the inverse shape of the mould. The tooling to produce these lenses is quite expensive, but it enables a low cost process that produces lenses in the thousands. Optical components made from plastics have the advantages of low weight, miniaturization, high performance, greater flexibility in surface shapes and reduced cost [87].

In contrast, glass offers advantages over plastics in optical characteristics such as refractive index range and index change with temperature. Although each material requires different production methods, they both actively contribute to progress in optical elements with high function and performance. Small lenses are moulded in glass using a method called precision glass moulding or PGM [182]. The lenses are formed into the final shape by being pressed into a die at high temperature. This method economically produces small spherical and aspheric optics in a variety of glasses, giving diffraction limited performance and excellent surface finish. These lenses are used in high-volume goods such as pocket cameras. Larger condenser lenses for projectors, which have less stringent requirements, are also made this way [2].

FISBA OPTIK has developed a lens array design for a beam twister made from a high index mouldable glass material. The shape of each single lens has to be aspheric. The requirements in terms of centre thickness, flatness and alignment of both high. For example, a pitch accuracy was achieved in the sub-micrometre range and the form accuracy of the final aspheric product was measured to be in the range of 0.1 μm rms [193].

One microlens array mould was fabricated, which is a fixed component in the focal region of a telescope. The high-speed wavefront sensor measures deterioration in wavefront due to air turbulence using part of light from a star. This lens array contains 188-microlens with radial arrangement. The development target was set to achieve 3.4 times greater resolution than the Hubble Space Telescope [174].

In plastic optics production, injection moulding and hot embossing involve high temperature and high pressure. They are time-consuming batch processes. UV curing optical cement is an adhesive which absorbs the ultraviolet (~254–378 nm) and quickly hardens to give a good bond. Due to the good optical performance (for example, the high index), UV curing polymers are also used in the production of optical micro systems and micro-optical elements. UV-moulding or UV-embossing produce high-quality optical elements in very cost-effective processes. This low pressure and low temperature process reduces cycle time. Tanigami et al. used UV-moulding to fabricate Fresnel microlenses on a glass substrate. The fabricated Fresnel microlenses had high temperature stability, low wavefront aberration, and diffraction-limited focusing characteristics [218]. Kunnavakkam et al. fabricated low-cost and low-loss microlens arrays using UV-moulding with an elastomeric mould [121]. Dannberg et al. integrated wafer-scale hybrid micro-optical subsystems such as vertical cavity surface emitting lasers (VCSELs) using UV photolithography [38].

Because the forming of UV-moulding is very fast, often in several seconds, roller embossing technology is rapidly emerging. In Fig. 43, the drum roller is used as the mould. During the roller embossing operation, the roller rotates around a fixed axis, while the platform slides underneath the roller. This operation increases the scale of production beyond what can be achieved by other methods [112]. The micro-structures are fabricated on the drum roller, which has a complex freeform surface. The fabrication of drum roller moulds needs the special machines with high rigidity and stability. The HDL-2000 from Moore Nanotech can produce the 2000 mm length micro-structured roller. Precitech makes a similar machine, Drum Roll 1400/450. Fabrication of micro-lens on drum roller was also studied using the fast tool control (FTC) unit as shown in Fig. 44 [69].

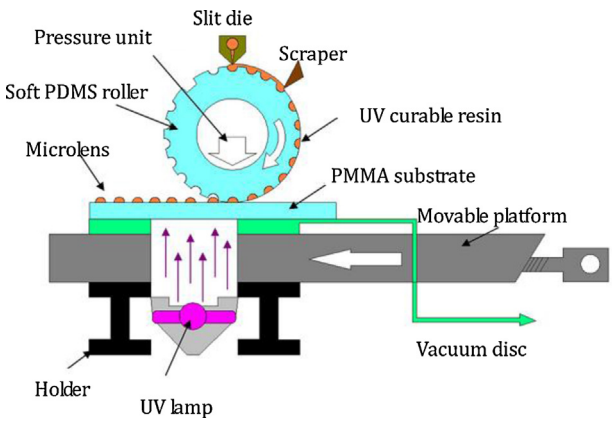

Fig. 43. UV-moulding using roller embossing [38].

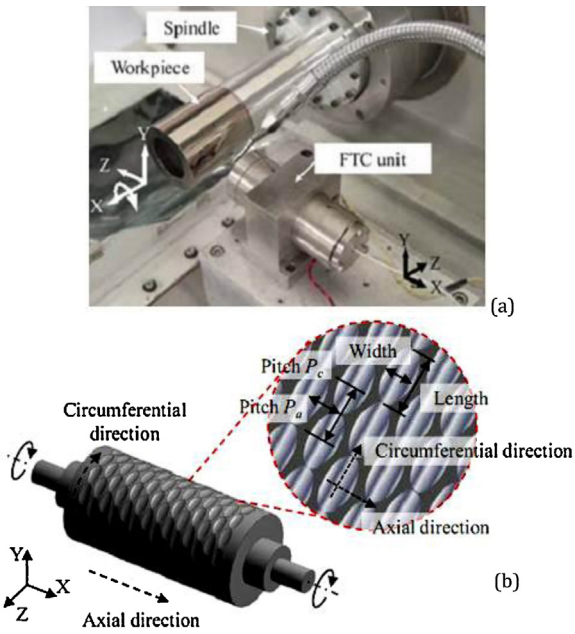

Fig. 44. Microlens on drum roller fabricated by FTC [69].

A piezoelectric force sensor was intergrated to measure the cutting force along the in-feed direction synchronously [69,125,163].

8. Measurements

Though ultra-precision machining can achieve a very high accuracy, many factors may cause the profile errors, such as environmental factors, machine structural errors, vibration and tool wear. The metrology and compensation are indispensable and fundamental techniques for obtaining better accuracy as shown in Fig. 4.

Savio et al. surveyed metrology for general freeform surfaces in 2007, ranging from car body parts to optics [191]. For optical surfaces, metrology requirements extend down to the nanometre range. Both contact (tactile) and non-contact measuring techniques are used, either offline and on-machine. Another way to discriminate the different measurement possibilities is between measurements with respect to a datum and those without any datum (e.g., for inspecting the form of a turbine blade without reference to the root profile).

Commercial instruments usually operate offline. The results contain systematic errors due to the machines error motions. Many instruments have small measuring range or long measuring time. On-machine metrology can avoid the errors caused by moving and re-positioning the workpiece. On-machine measurements can use the machine axes to extend the measuring range and improve the measuring efficiency. In this case, however, the systematic errors of the machine may be hidden.

8.1. Contact measurement

Currently coordinate measuring machines (CMM) are the most frequently applied instruments for measuring freeform parts in contact mode. Conventional CMMs have a large measurement range but an uncertainty in the micrometre range. Some studies were made to improve the precision of CMMs by applying laser interferometers, fulfilling Abbe's principle in all axes and fundamental principles of precision machine design [195]. Examples appropriate for measuring freeform optics include nanoCMMs from IBS, SIOS, Werth Messtechnik [100], as shown in Fig. 45. They can be characterized by a measurement range between 25 mm × 25 mm × 5 mm and 400 mm × 400 mm × 100 mm, a resolution in nanometre or sub-nanometre range and a measurement uncertainty in the sub-micrometre down to few-nanometres. However, the tactile probing mode requires slow scanning speeds and has the risk of damaging the surface. The measurement speed of these machines is limited in the range from some nm/s to about 1 mm/s.

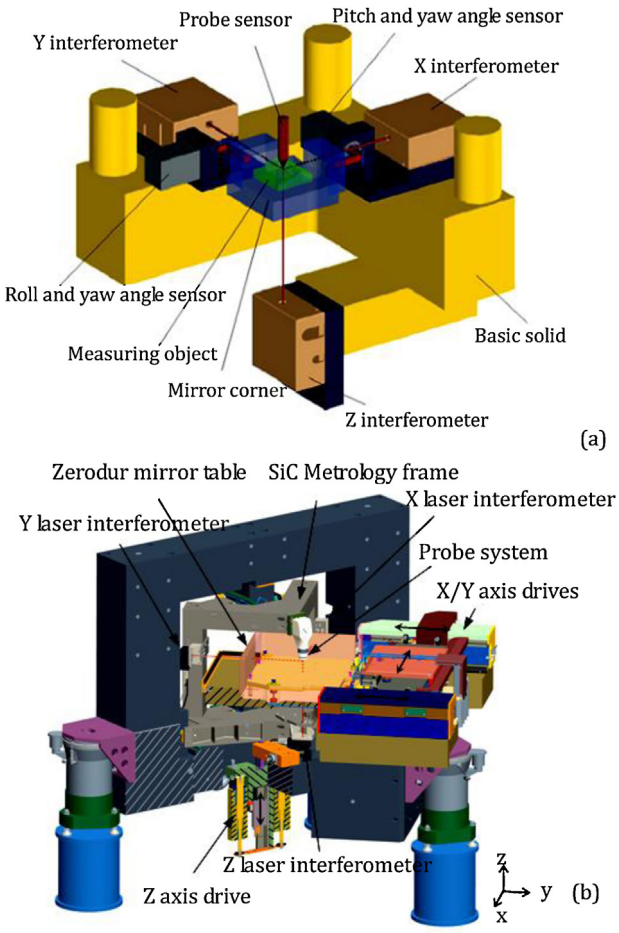

Fig. 45. Nanometric CMM. (a) SIOS and (b) IBS Isara 400.

The probe is the important sensor for CMM. The tactile 2.5D probes, so-called profilometers such as the products of Taylor Hobson, are widely used. Their principle and operation is well known and standardized, e.g., ISO 3274. The surface is scanned with a conical or pyramidal shaped tip made of ruby or diamond [240] and is suitable for the rotationally symmetric lenses. For freeform optics microtactile 3D probes play an important role; such probes are similar to conventional tactile systems based on CMMs, but with resolution and accessibility of small features. One such micro-probe is the "Triskelion" system by IBS (Fig. 46), based on an earlier design of the NPL and used mainly in the IBS Isara. Its

Fig. 46. "Triskelion" probe in the Isara 400 [241].

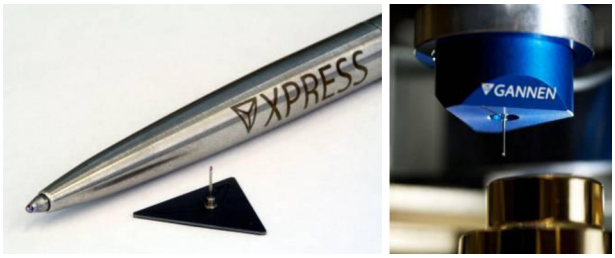

Fig. 47. Probe system Gannen XP.

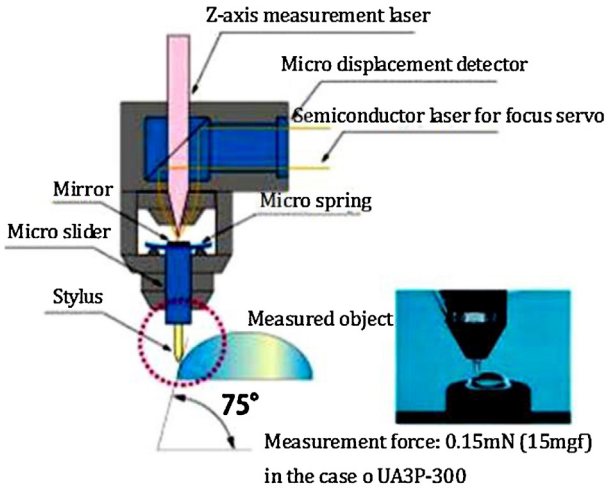

Fig. 48. Contact mode nanometric CMM.

force sensors consist of three capacitive sensors. The moving target discs of the sensors are suspended by flexure hinges and connect to the stylus in the centre. With the capacitive signals the stylus deflection in X, Y and Z is calculated. The stylus consists of a stiff tungsten carbide shaft with a small ruby sphere ($\varnothing$ 0.5 mm) at the end. Except for the sensors, the stylus and the probe tip, the complete probe is made from invar to ensure good thermal stability [44,241].

Another design was developed at the TU Eindhoven and is now available by Xpress, the "Gannen XP", as shown in Fig. 47 [78]. It is based on piezoresistive deflection detection, allowing a far higher sensitivity than regular resistive strain gauges. The stylus is connected to a triangular silicon membrane suspended by three small strips containing the strain gauges. The membrane and the sensors are manufactured in one piece by the means of micro-system technology manufacturing processes allowing a low moving mass of 25 mg. Several designs have been developed trying to scale down regular tactile 3D probes [7,131]. Other approaches avoid the need of a defined probing force by directly registering the deflection of a very soft stylus optically or by changes in the amplitude of vibrating probe tips [84,180]. An overview of available probing systems can be found in [233,236,238].

Apart from classical profilometers with a specialized axis setup, more designs use a CMM as basis and at least partially incorporate the Abbe principle. For instance a profilometer head was installed in the NMM-1 system [140]. Due to lack of rotational axes the accessible surface angle in measurements with nanoCMMs is limited. A alternative is a combination of the Cartesian setup of the CMM with a polar setup. A point sensor is mounted on two rotary axes, which are stacked under an angle of 45°. The sensor tip coincides with the centre of both rotary axes and can be tilted around its working point, as Schuler reported [238]. The freeform workpiece is positioned underneath the polar setup on a triaxial scanning stage. During measurement the sensor is rotated to stay perpendicular to the local surface slope. During the scanning movement systematic alignment and guidance deviations of the polar system are compensated with the control of translation stage. The effectiveness of dynamic sensor rotation is shown in simulation [239] and in practice with a prototype, based on the mentioned CMM of SIOS [199].

Contact trigger probes have been used to detect the surface to be measured, since the orthogonal setup makes the application of an optical non-contact probe difficult for surfaces with large slopes. An atomic force probe, according to the manufacturer, is used as shown in Fig. 48 in combination with interferometers and stationary reference mirrors. The probe is kept at a constant distance from the surface, resulting in a "semi-contact "measurement. A vertical interferometer is employed to measure the vertical displacement of the probe relative to a horizontal reference mirror. In addition, it can measure the slopes of surface up to 75°. Although the surface is not in contact, scanning speeds are still limited to 5 mm/s, leading to measurement times of many hours for large surfaces [215].

Scanning Tunnelling Microscopy (STM) and Atomic Force Microscope (AFM) are the important techniques to measure micro-structured freeform optics. Although they are nominally non-contact, they work in the scanning mode similar to CMM system. STM is based on a electrical near-field interaction with a conductive surface, the quantum effect tunnelling current [14]. The probes are wire tips with a tip radius of single nanometres. AFM uses sharp cantilever tips also with a curvature of a few nanometres and, depending on the mode of operation, is in contact with the surface or keeps a distance of a few nanometres being attracted by surface forces [39]. Both principles are non-contact or apply a negligible force. They offer a lateral resolution in the nanometre range and vertically sub-nanometre. The disadvantages are limitations in the working range and the long time needed for scanning. A variety of research institutes have integrated AFMs into longer range scanners or CMMs. For most commercially available systems, the lateral working range is usually in the range of a few tens of micrometres and the vertical range even less. Therefore scanning probe systems can only investigate small parts of a surface. To keep the measurement time low, a feature-oriented measurement strategy is necessary. With high resolution, they are an important tool to support other measurement, such as with local feature and roughness measurements. A feature-oriented measurement strategy was presented for measurement time reduction. This method optimizes the measurement operations, enabling the selection of higher resolutions where needed [141,192].

8.2. Non-contact measurement

Optical surface measurement methods (including imaging) and interferometric techniques provide non-contact measurement of freeform optics, and may measure the entire surface in a single measurement. Optical measurements can be performed very fast and with low uncertainty, but are sensitive to environmental influences as well as to disturbances caused by the workpiece itself (colour, roughness, defects, chips from machining, dust, oil or water coats, etc.). Accuracy normal to the surface can be excellent in interferometric procedures; lateral resolution is limited by diffraction (i.e., the Rayleigh criterion). The limiting angular resolution θ between two still discernable points is given by $\sin\theta = 1.22\ \lambda/D$, where D is objective diameter and λ the wavelength. The application of optical sensors can be limited by the required reflectivity and the required range for the angle between surface and beam. Further limits can arise from certain surface structures like steps or high surface curvature. Steps can lead to optical edge artefacts, so-called batwings and high surface curvature, in some interferometric systems can lead to phase jumps, or so-called ghost steps [68,123].

Interferometry is a well known solution for fast measurement of surfaces with sub-nanometric resolution in the direction of

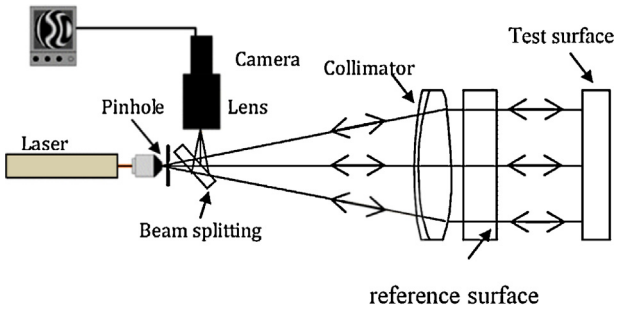

Fig. 49. Laser Fizeau interferometer.

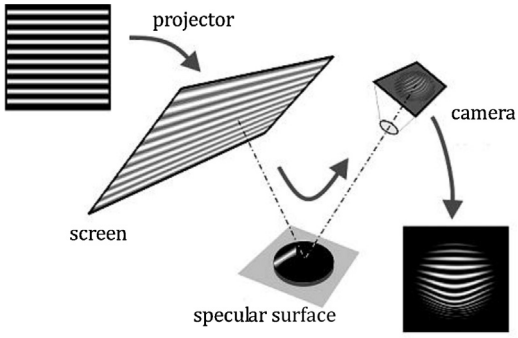

Fig. 50. Phase measuring deflectometry [186].

beam propagation [45,244]. In most cases, the Fizeau configuration is most suitable because it employs the least number of components and can be accomplished with relative small residual system errors. An interferometer (Fig. 49), combines the reflected wavefront of a reference surface and the wavefront coming from the surface to be measured. The distance between the fringes of the interferogram represents exactly one wavelength optical path difference between the beams, and thus half a wavelength departure between the reference surface and the surface to be measured. The entire surface is imaged at once, measuring it in seconds without contact. The technique has been available as a commercial tool since the early 1970s and a number of well respected manufacturers such as Zygo, Veeco, have made them over the years. An extensive overview of many interferometry based techniques is given in [138]. High accuracy of measurements can be achieved using a technique known as phase shifting, and the direction of the height difference can be derived accurately and automatically.

Laser interferometers are ideal for measuring flat and spherical surfaces with a matching reference. When measuring an aspheric or freeform with too much deviation from the reference wavefront, the reference can be matched to the surface under test by using a correction element such as a null lens or Computer Generated Hologram (CGH). The reference can be a diffractive optical element manufactured by high precision lithographic methods. These elements have to be specially designed and manufactured for each specific surface shape. CGHs have limited dynamic range and are not practicable for all freeforms. In addition, alignment is a very important issue, as it is a calibration of the CGH [27,150].

When the deviation between the reference and test surface increases, the number of fringes increases as well. With a $1k \times 1k$ CCD, up to a few hundred fringes can be resolved, which limits the slope of local deviation from spherical. One way to reduce the number of fringes on the detector is by decreasing the aperture. By imaging multiple sub-apertures of the surface, and numerically stitching these together, a complete surface area measurement can be obtained. A number of different groups have used stitching techniques as a way to address the aperture size or aspheric departure, dating from the 1970s or before. The work at QED is one example [47]. When the deviation is in the order of millimetres, the amount of sub-apertures that is required increases rapidly, along with the measurement time.

Stitching errors increase rapidly with the number of sub-apertures. A number of techniques have been developed using slope or curvature, such as Traceable Multi Sensor (TMS) technique, which measures freeform surface using interferometer sensor in scanning style. An autocollimator is applied to conduct tilt measurements of the sensor system at each scanning position [74,252].

Phase Measuring Deflectometry (PMD) is a cost-effective and robust system for measuring freeform surfaces. In this method, sinusoidal fringes are projected onto a surface. The surface variation causes fringe variations, as recorded by a camera (Fig. 50). By phase-shifting the fringes, the surface profile and curvature can be deduced. This method has been applied for progressive spectacle glasses. It was also used to measure X-ray mirror with the better than 100 nrad (rms) precision of surface slope errors [209]. PMD focuses onto the object and the fringes at the different time so that it is not limited by the intrinsic depth of field [186,226]. Similarly, in the Fringe Reflection Technique (FRT) the variation in fringes spacing is converted to, local gradients for each camera pixel. This method is less sensitive to external vibrations and temperature instabilities. A multi-facet mirror machined by fly-cutting was measured, presenting a lateral resolution of 70 μm and nanometer vertical resolution. Despite the high resolution of the system, the height of the investigated surface may range within several 10 mm [16,75].

An auto focus laser probe mounted on CMM can measure freeform optics in non-contact mode. Fig. 51 shows an example using this method. With the laser beam focused on a sample surface using the microscope objective lens, the surface reflected light is detected by a four quadrant detector (FQD). The *Z*-axis surface position of sample is detected by an AF (auto focus) sensor [54]. The XY position is scanned with a high-precision mechanical stage controlled by the optical linear control system. A machine in 4° of freedom was also developed, in which the position of the probe relative to the lens can be measured, as shown in Fig. 52 [80,81].

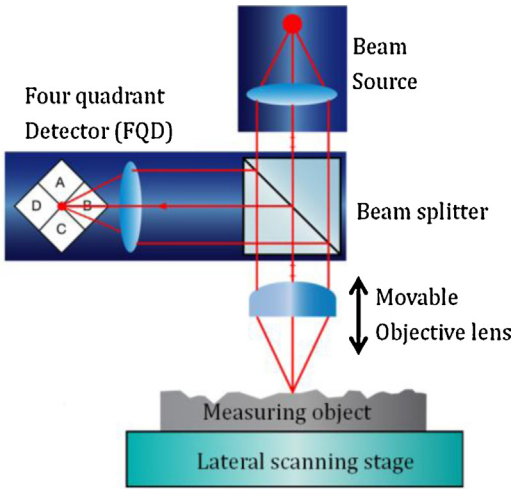

Fig. 51. CMM with auto focus sensor [54].

Confocal microscopy is an effective tool for profile measuring at micro-scale. The maximum detectable slope is higher than other instruments, and can reach 75° with enough scattered light [144,191]. Data are typically much noisier for high slopes. Chromatic confocal scanning has been suggested for freeform

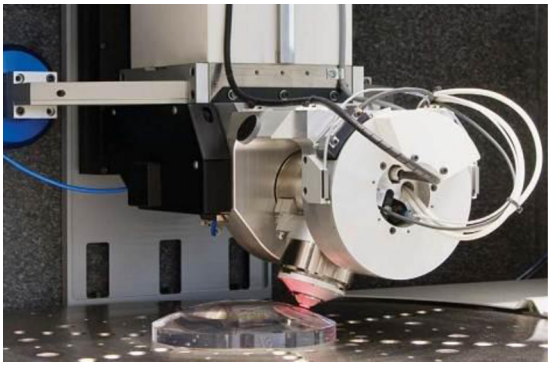

Fig. 52. 4-degree CMM with auto focus sensor [80].

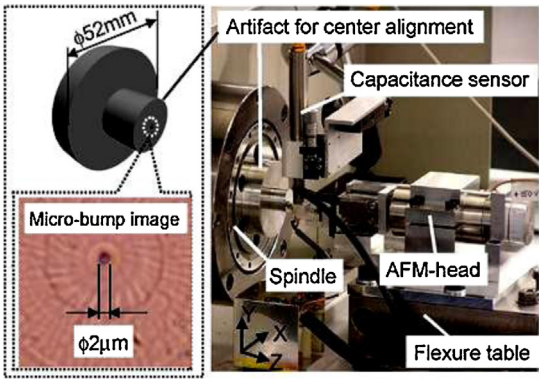

Fig. 54. AFM-head on turning machine [70].

microparts. But as the point scanning of the whole surfaces takes a long time, a feature-oriented reduction to representative single profiles is suggested [107].

8.3. On-machine measurement

In on-machine, or in situ measurement, an appropriate probing system is built into the ultra-precision manufacturing machine, moved by the machine axes, and provides measurement data without removing the workpiece from the machine. The measuring range of the original measuring system is extended by the machine axes and the measuring path can be controlled using the CNC machine. Typically point to point scanning is used in these current On-machine measurements.

Moore Nanotech provides the Workpiece Measurement and Error Compensation System (WECS) for on-machine metrology in which an air bearing LVDT probe is mounted onto the ultra-precision turning machine (Fig. 53). The probe moves along the ideal measuring path under control of *X*, *Z* axes, while Linear Variable Differential Transformer (LVDT) sensor captures the position deviation of probe due to the figure error of measured surface. This system provides the compensation of shape errors with the filtering operation.

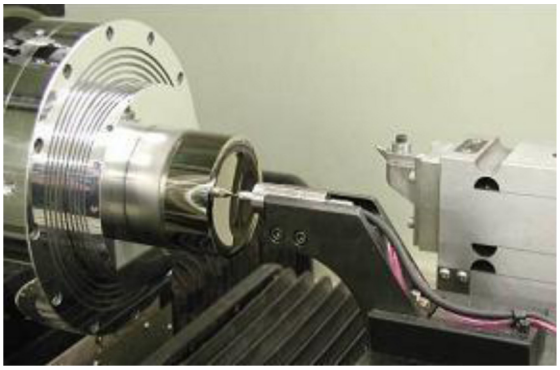

Fig. 53. WECS using the LVDT probe [courtesy of: Moore Nanotechnology Systems].

A number of variants of this approach have been used. One great advantage is that the air bearings allow the probe to move freely in the direction of workpiece, while provide high stiffness laterally. Probe displacement can be measured by a variety of techniques, including interferometery, which allows high resolution over large ranges [161].

In on-machine measurement, another significant error source is the alignment error between the spindle rotation axis and the probe tip of the contact-type displacement sensor, or the centering error. Shibuya et al. proposed a spiral scanning probe measurement system, including a method to make the alignment accurately. They reported results of experiments of surface profile measurement of a micro-aspheric lens.

Other approaches include mounting a contact-type displacement sensor on a slide, with a ring artefact vacuum-chucked on the spindle surrounding the aspheric object, and two capacitance-type displacement sensors set on the slide to scan the surface of the ring artefact [203]. The surface profile of the ring artefact can be measured accurately by reversal [53]. Three sensors can be applied to measure the motion errors of the probe completely.

A conventional atomic force microscope (AFM) has a very small measuring range. However, Gao et al. mounted an AFM cantilever tip on a diamond turning machine, and a linear encoder with a resolution of 0.5 nm for accurate measurement of the *Z*-directional profile height in the presence of noise associated with the diamond turning machine (Fig. 54). A superposition of periodic sine-waves along the *X* and *Y* directions (wavelength (*XY*): 150 μm, amplitude (*Z*): 0.25 μm) were measured [70].

In freeform grinding machines, on-machine measurement is applied widely. Satisloh integrates the On-Machine-Metrology (OMM) in their CNC grinders. The sensor is built into the tool head of a CNC machine, moved by the CNC-axes. Besides high resolution capability, this setup enables measurements with the work piece in the same position, where it is machined, i.e., without the necessity to move or re-position the work piece. OMM offers a resolution of 0.1 μm on ground surfaces, limited by the systematic machine errors.

White light interferometer systems combine proven non-contact measurement technology, delivering over 1 million data points at sub-Angstrom resolution, with a set up boasting simple integration, good vibration immunity and very simple software control. White light interferometers have been designed for integration into automated production line metrology applications both on-machine and in-line [233,236].

There are a number of different probes that can be integrated into different machines providing trade-offs between resolution normal to the surface, lateral resolution, speed, and noise. An example was developed using laser probe unit with a maximum resolution of 1 nm, a measuring range of 10 mm, a repeatability of 5.6 nm and a maximum measurable angle of 60° [167].

9. Characterization

Characterization of freeform optics commonly requires the integrated technologies of alignment (also called matching or registration), stitching procedures (in special cases), filtering and traceability as well as characterization/verification. The general principle of form evaluation of freeform surfaces is to align extracted points (from the measured data) and design data (CAD-model of nominal form) and to evaluate the deviation between them. For alignment the measured point cloud describing the real surface is transformed (rotated and translated) to best fit either

- to the nominal reference coordinate system, defined in the CAD-model by a datum system consisting of standard features like plane, cylinder, etc. (ISO 5459), or
- directly to the nominal (theoretical) CAD-model of the freeform surface. In this case the alignment consists of coarse and fine registration procedures as described in [235]. Non-linear optimization methods are applied for optimizing the alignment. For characterizing the quality of the registration least square or minimum zone criteria are used [234,237].

Surface parameters, such as Ra for roughness and PV for form error, have long been used. Such parameters have significant limitations in surface characterization [50]. For 3D freeform surface, these characterization parameters are particularly defective. Other mathematical methods are being used to characterize the measured surface, for example Fourier transforms and autocorrelation [15]. Currently, the standard ISO 25178-2 is being developed and some parts published; this standard is related to the analysis of 3D areal surface texture, including height, functional, spatial, hybrid and feature parameters [91]. Spatial characterization over a broad range of spatial separations is an active research topic.

9.1. Alignment

Before applying alignment methods the collected points must be corrected for known systematic deviations of the measuring system. This includes – for tactile CMM measurements – probe stylus bending effects and the tip ball correction caused because the centre point of the tip ball is captured but the surface point is different. The probing direction (probing vector) relative to the normal direction on the freeform surface has to be considered for correction of the point differences. For optical measurement systems optical distortions in the optical path must be corrected as far as possible before application of alignment procedures. Systematic errors like form deviation and wear of the probing tip, have also to be corrected in scanning probe systems. All other systematic effects must be considered [78]. After correcting known systematic point deviations further processing of the data can be done. The first step is alignment.

There are two main methods to align freeform surfaces. The first considers functionally relevant surfaces to define the workpiece coordinate system which is then transformed to the reference coordinate system of the designed surface. The other aligns both surfaces considering all data points, applying either surface or feature based approaches. The form error is obtained from the distance from the measured points to the designed surface. After filtering, reliable characterization results are derived if the influence of systematic errors is eliminated efficiently. Jiang et al. described the data processing technology for 3D surface metrology [106].

After obtaining the measured data, a non-linear coordinate transformation must be solved in order to ensure the consistency of the measured coordinates with the designed coordinates by matching methods. Freeform matching is an optimization process. The iterative closest point (ICP) algorithm has been adopted to carry out the surface matching process. ICP algorithm and rigid body transformation based on mean-square distance have been used for 3D shapes registration [13,183,201]. Some studies have been undertaken to improve the efficiency of the ICP. For example, Ravishanker used a modified ICP with a priori knowledge of two point sets between measured and model [185]. Liu proposed a method which manipulated possible point matches established by ICP criterion based on colinearity and closeness constraints [134].

Jiang et al. introduced a structure neighbourhood signature fitting method for smooth freeform surfaces and tessellation technique to identify and characterize micro-structure surfaces. The method applied an inscribed sphere within the boundaries of the measured surface to obtain the intersection curves and fitting plane inside the sphere, to find correspondent features in templates. Fine alignment was conducted by using the Levenberg–Marquardt algorithm [103].

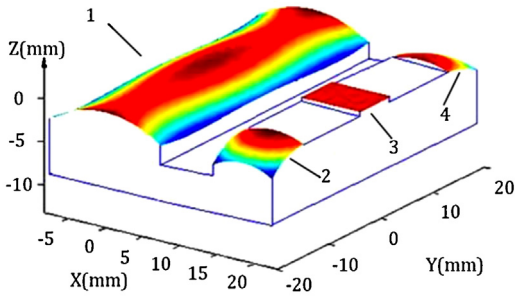

Fig. 55. Surface alignment with CRD method [118].

Kong et al. proposed the coupled reference data method (CRDM) to evaluate smooth optical freeform surfaces with high efficiency and precision. The coupled reference data (CRD) are designed around the workpiece and machined together with it, as shown in Fig. 55, where surface 1 is the workpiece and surfaces 2, 3, and 4 are the reference surfaces. By aligning the reference data, the proposed CRDM carries out fast surface matching. This makes good preparation for the next matching optimization which is conducted by the least-squares and minimum zone method. The optical *f*-theta workpiece was measured and evaluated [118].

One promising matching approach is the utilization of the surface intrinsic properties, which is independent from the coordinates. In essence, CRDM provides additional features manually. Seeger et al. presented an overview of rigid registration methods applicable to surface descriptions by feature extraction and registration technology. The types of freeform features are formally described by means of an analytical definition for the surface modification through deformation and eliminations laws utilized two intrinsic surface properties, the Gaussian and the mean curvatures, as object features for matching [200]. Lines of equal curvature were used to establish the relationship between two objects and the matching was realized by interval projection polyhedron algorithm and rigid body transformation. Ko et al. utilized two intrinsic surface properties, the Gaussian and the mean curvatures, for surface matching, and the related iso-curvature lines were employed to establish the correspondence between two objects [113,114]. Kase et al. applied the main curvature changes of the measured and designed surface to conduct local characterization while the global characterization was carried out based on the normal vector [110].

Cheung et al. used the Gaussian curvature for data matching. A smooth aspheric surface and a micro-structured surface were evaluated, showing that the proposed method is more robust than traditional matching criteria. Fig. 56 shows the Gaussian curvature distribution of measured lens array and the reported form error [34].

There are also some software packages available in the market, such as Polyworks, RapidForm, Imageware and Geomagic, providing the comparison procedures including the manual initial alignment, suggestions for the registration operations of systems and feature-based alignment. Although some research and achievements in measurement of freeform surfaces have been reported, most of them are still limited to the millimetre or micro/sub-micro metre scale due to the matching precision. Therefore, the acquisition of form error data by on-machine metrology has advantages. For example, the WECS of Moore Nanotech gives the form error directly. Some research evaluating the optical properties avoids the shape evaluation because of the matching difficulty [155,173]. Nussbaum et al. characterized the surface profile and the wave aberration as well as the surface roughness [164]. Some parameters such as microlens pitch, fill factor, surface quality, and wavefront quality have been examined for lens-let arrays for astronomical spectroscopy by Lee and Haynes [124].

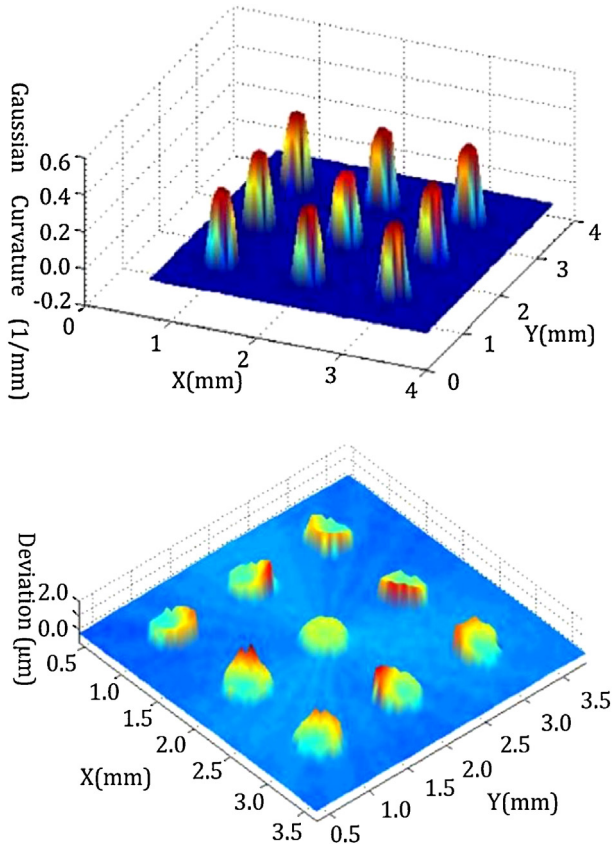

Fig. 56. Gaussian curvature (above) and form error (below) [34].

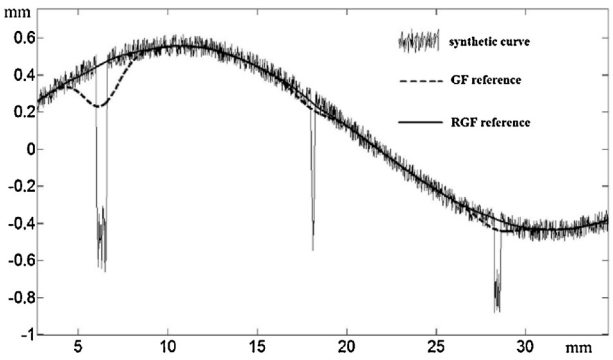

Fig. 57. Filtering results compared by common and robust filter.

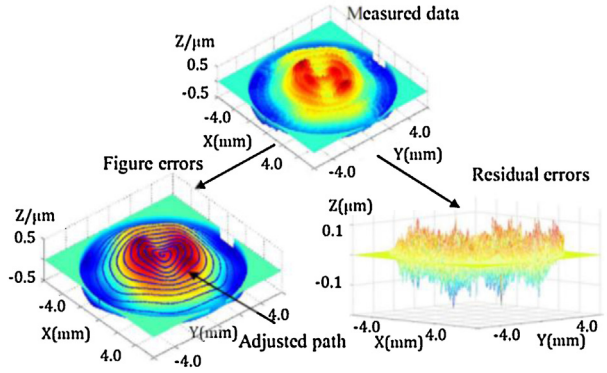

Fig. 58. Process example for turning and compensation.

If the measured objects are bigger than the measurement area of the sensor used, surface data can be captured with shifted sensor positions. After each measurement the object is relocated and an additional measurement made which overlaps with the previous measurement. Next all the individual measurements are combined to one surface description (stitching). For the coarse registration the calibrated sensor-positions are applied [109]. Depending on the positioning accuracy of the positioning stage the result can be improved during fine registration [143]. The process of stitching gives data over larger measurement areas with higher spatial resolution and can capture higher slope angles by moving the sensor position accordingly [142].

9.2. Filtering

The form errors obtained by matching can be used for shape compensation to reduce the deviation, because they contain the roughness, waviness and real form deviation. Three components should be separated using the filtering methods, which have been widely discussed [for example 104–106, 127, 179]. The earliest filter used in surface metrology is the 2RC filter [4]. Owing to the advantage of correct phase with a minimum time–frequency window area, Gaussian filtering (GF), rather than 2RC, is now recommended as the default method for characterizing surface topography [99]. Wavelet analysis decomposes the surface data into multi-scalar space. By transferring space-based information into scale-based information, it can identify not only frequency events of the original data but also their location properties can be kept. Many new breakthroughs and research trends in surface characterization have been reported, such as robust filtering, the Motif and fractal method [90–97]. However, despite their certain merits, these nascent methods are restricted in practical application. ISO/TC 213 is currently taking up review and comments of integration of these filters into the international standards.

Filters that are not robust can produce a distorted estimate of underlying form, due for example to the effect of the tool marks on the machined surface or outliers. This distorted form would result in incorrect shape compensation. Therefore, 3D robust filters remain an active topic of research [93,127,231]. Fig. 57 shows a comparison of a GF and robust Gaussian filtering (RGF); the RGF is more effective in the presence of outliers. Fig. 58 gives an example of compensation of turning after filtering, showing the real figure error and residual error. The adjusted path for compensation is generated based on the figure error data.

Filtration on complex freeform geometries at the micro-nano scale is very challenging since current standard filters mentioned above are based on planar method that leads to distortion when applied to freeform surfaces. An initial investigation into the use of mean curvature motion (MCM) for the smoothing of freeform surface has been reported [102,106]. This uses Partial Differential Equations (PDE) to provide a generalization of 'Gaussian filtering' to freeform surface without distortion.

9.3. Traceability

Traceability is often considered one of the desiderata of modern metrology and seen, often erroneously, as an endorsement that the measurement is of the highest quality. If the goal of the measurement is process control, traceability may not be necessary, provided that there is a relationship between the measurements made and the function of the product or process.

Traceability is defined as a property of the result of a measurement whereby it can be related to stated references through an unbroken chain of comparisons all having stated uncertainties [89]. This has three significant consequences. First, only measurements that can be made by the National Metrology Institutes (NMIs) can be traceable; second, that uncertainties must be properly propagated through the chain of comparisons; and third that the accumulation of uncertainties through the comparisons does not overwhelm the functional requirements of the measurement.

For many measurements requiring traceability, the conventional chain of comparisons is perfectly adequate. Few freeform optics can be measured at NMIs. There is another route to traceability according to the requirements of ISO 17025 [3]. According to the US standard on metrological traceability [4], metrological traceability is always to the unit; an appropriate metrological terminus can be a competent laboratory or a realization of the SI metre. This recommendation is reinforced in ISO 17025 which states that traceability to SI units may be achieved by reference to a natural constant, the value of which is known and recommended by the International Committee of Weights and Measures (CIPM). CIPM recommendations for standard frequencies and for the practical realization of the metre appear on the BIPM website, provided that the given specifications and accepted good practice are followed.

A claim of traceability, following this second route, for a derived quantity (e.g., departure from the designed shape) requires a rigorous uncertainty analysis. This has been documented, in the case of optical flats [51] based on a NIST memorandum [146] which states "...the three flat method is used at NIST to calibrate our master reference flats, the method is very well documented in the technical literature, and provides adequate traceability to satisfy the requirements of ISO 17025". The same approach to traceability through realization of the unit and rigorous uncertainty analysis and cross-checking might be taken to measurements of freeform surfaces.

10. Conclusions

Manufacturing of freeform optics is a promising technology in various applications discussed in this paper. The manufacturing of freeform optics requires integrating multiple technologies including design, machining, metrology and evaluation. For the design of freeform optics, multi-parameter optimization has been adopted widely using various commercial software systems. However, the direct mapping method has potential for higher accuracy design, although it still depends on a fitting model method with high accuracy because the discrete points are directly calculated. In design of freeform optics, the tolerances should be a key focus, in order to reduce the precision requirement of machining. Machining method is the core technology of freeform optics, facing several important problems currently as follows.

- More types of complex surfaces are necessary to be machined in many applications.
- More types of materials need to be machined efficiently using the diamond turning, milling, grinding and polishing methods to meet the demanding requirements.
- The machining accuracy of freeform optics is expected to be improved to nanometer or even sub-nanometer scale.

The first two issues can be resolved by new configurations and new processes. The third issue requires new devices or systems with better accuracy, in which the tool path is designed through analysing the kinematics of machining comprehensively. Freeform optics is a developing technology; design, machining, moulding, measurement, characterization and standardization remain research topics. The mathematical models for freeform geometric specification and verification are still in the early stage of research. New instrumentation and methods, artefacts, uncertainty analyses and reference algorithms will be important next steps towards traceable freeform measurement. The on-machine method to measure the form errors directly can be used to avoid the matching process through using the high-precision displacement sensors with a short measuring range, provided systematic errors are properly treated. In addition, the measurement of optical performance should be considered as this is key to eventual applications.

Acknowledgements

Acknowledgements to the following persons for their contributions:

- Oltmann Riemer, Laboratory for Precision Machining LFM, Bremen, Germany.
- Xiangqian Jiang, University of Huddersfield, Centre for precision technologies, UK.
- Benny C.F. Cheung, Advanced optics manufacturing centre, Hong Kong Polytechnic University, Hong Kong, China.
- Wei Gao, Department of Nanomechanics, Tohoku University, Japan.
- Eckart Uhlmann, Fraunhofer-Institute for Production Systems and Design Technology IPK, Germany.
- Leonardo De Chiffre, Centre for Geometrical Metrology, IPL – Technical University of Denmark, Lyngby, Denmark.
- Henny A.M. Spaan, IBS Precision Engineering, Netherlands.
- Enrico Savio, DIMEG, University of Padova, Italy.
- Don A. Lucca, Oklahoma State University, USA.
- Harald Bosse, Physikalisch-Technische Bundesanstalt (PTB), Germany.

The authors thank Y. Cheng, Y.H. Nie, F.F. Xu and X.L. Liu for their supports in searching relevant publications. The gratitude is also expressed to A. Schuler and L. Shaw for contributions to the sections 8 and 9. The acknowledgements are extended to the supports of the State Key Program of Basic Research of China ("973" Grant No. 2011CB706703), and the National Natural Science Foundation of China (Grant No. 90923038).

References

[1] Álvarez JL, Hernández M, Benítez P, Miñano JC (2001) TIR-R Concentrator: A New Compact High-gain SMS Design. *Proceedings of the SPIE* 4446:32–40.
[2] Anderson D, Burge J (2001) *Optical Fabrication, Chapter 28 in Handbook of Optical Engineering*, CRC Press.
[3] ANSI/ISO/IEC 17025(E) General requirements for the competence of testing and calibration laboratories.
[4] ASME B.89.7.5-2006, Metrological Traceability of Dimensional Measurements to the SI Unit of length http://www.bipm.org/en/publications/mep.html, (accessed 01.29.13).
[5] ASMEB46.1 (1995), Surface texture (surface roughness, waviness and lay), 1–98.
[6] Atad-Ettedgui E, Peacock T, Montgomery D, Gostick D, et al (2006) Opto-mechanical Design of SCUBA-2. *Proceedings of the SPIE* 6273:62732H.
[7] Balzer FG, Hausotte T, Dorozhovets N, Manske E, Jäger G (2011) Tactile 3D Microprobe System with Exchangeable Styli. *MST 22 id 094018*.
[8] Bäumer S (2005) *Handbook of Plastic Optics*, Wiley-VCH Verlag GmbH & Co. KgaA.
[9] Belousov AA, Doskolovich LL, Kharitonov SI (2008) A Gradient Method of Designing Optical Elements for Forming a Specified Irradiance on a Curved Surface. *Journal of Optical Technology* 75(3):161–165.
[10] Benítez P, Miñano JC (2007) The Future of Illumination Design. *Optics and Photonics News* 18(5):20–25.
[11] Benítez P, Miñano JC, Blen J, Mohedano R, et al (2004) Simultaneous Multiple Surface Optical Design Method in Three Dimensions. *Optical Engineering* 43:1489–1502.
[12] Benitez P, Miñano JC, Blen J, Mohedano R, et al (2004) SMS Design Method in 3D Geometry: Examples and Applications. *Proceedings of the SPIE* 5185. http://dx.doi.org/10.1117/12.506857.
[13] Besl PJ, Mckay HD (1992) A Method for Registration of 3-D Shapes. *IEEE Transactions on Pattern Analysis and Machine Interlligence* 14(2):239–256.
[14] Binnig G, Rohrer H, Gerber C, Weibel E (1982) Surface Studies by Scanning Tunneling Microscopy. *Physical Review Letters* 49(1):57–61.
[15] Blateyron F (2006) New 3D Parameters and Filtration Techniques for Surface Metrology. *Technology Report of Digital Surf*, www.digitalsurf.fr/en/index.html.
[16] Bothe T, Li W, Kopylow C, Juptner WPO (2004) High-resolution 3D Shape Measurement on Specular Surfaces by Fringe Reflection. *Proceedings of the SPIE* 5457:411–422.
[17] Bradby JE (2003) In situ Electrical Characterization of Phase Transformations in Si During Indentation. *Physical Review B* 67:085205.
[18] Brecher C, Lange S, Merz M, Niehaus F, et al (2006) NURBS Based Ultra-precision Free-form Machining. *CIRP Annals – Manufacturing Technology* 55(1):547–550.
[19] Brinksmeier E, Autschbach L, Weck M, Winterschladen M (2004) Closed Loop Manufacturing of Optical Molds Using an Integrated Simulation Interface. *Proceedings of 4th euspen International Conference Glasgow, Scotland*, 215–217.

[20] Brinksmeier E, Gläbe R, Flucke C (2008) Manufacturing of Molds for Replication of Micro Cube Corner Retroreflectors. *Production Engineering* 2(1):33–38.
[21] Brinksmeier E, Mutlugünes Y, Klocke F, Aurich JC, Shore P, Ohmori H (2010) Ultra-precision Grinding. *CIRP Annals – Manufacturing Technology* 59(2):652–771.
[22] Brinksmeier E, Riemer O (2010) Submicron Functional Surfaces Generated by Diamond Machining. *CIRP Annals – Manufacturing Technology* 59(1):535–538.
[23] Brinksmeier E, Riemer O, Gessenharter A, Autschbach L (2004) Polishing of Structured Molds. *CIRP Annals – Manufacturing Technology* 53(1):247–250.
[24] Brinksmeier E, Riemer O, Osmer J (2008) Tool Path Generation for Ultra-precision Machining of Free-form Surface. *Production Engineering* 2(3):241–246.
[25] Brückner A, Duparré J, Leitel R, Dannberg P, et al (2010) Thin Wafer-level Camera Lenses Inspired by Insect Compound Eyes. *Optics Express* 18:24379–24394.
[26] Bryan, J.B., 2006, System and method for forming a non-rotationally symmetric portion of a workpiece, US Patent 7089835 B2.
[27] Burge JH, Wyant JC (2004) Use of Computer Generated Holograms for Testing Aspheric Optics. *Proceedings of the SPIE* 5494:45–50.
[28] Cakmakci O, Moore B, Foroosh H, Rolland JP (2008) Optimal Local Shape Description for Rotationally Non-symmetric Optical Surface Design and Analysis. *Optics Express* 16(3):1583–1589.
[29] Cakmakci O, Vo S, Thompson KP, Rolland JP (2008) Application of Radial Basis Functions to Shape Description in a Dual-element Off-axis Eyewear Display: Field-of-view Limit. *Journal of the Society for Information Display* 16(11):1089–1098.
[30] Chapman G (2004) Ultra-precision machining systems; an enabling technology for perfect surfaces. *Moore Nanotechnology Systems*. http://www.nanotechsys.com/technology/technical-papers/.
[31] Chen WK, Kuriyagawa T, Huang H, Yosihara N (2005) Machining of Micro Aspherical Mould Inserts. *Precision Engineering* 29:315–323.
[32] Cheng DW, Wang YT, Hua H, Talha MM (2009) Dedsign of an Optical See-through Head-mounted Display with a Low f-number and Large Field of View Using a Freeform Prism. *Applied Optics* 48(14):2655–2668.
[33] Cheng Y, Hsu W, Chen Y, Su G, et al (2010) Design and Fabrication of Free-form Shaped Lens for Laser Leveler Instrument. *OSA Technical Digest (CD)* FThX2.
[34] Cheung CF, Kong LB, Ren MJ (2010) Measurement and Characterization of Ultra-precision Freeform Surfaces Using an Intrinsic Surface Feature-based Method. *Measurement Science and Technology* 21:115109.
[35] Clayor NE, Combs DM, Lechuga OM, Mader JJ, et al (2004) An Overview of Freeform Optics Production. *Proceedings of the SPIE* 5494.
[36] Clayor NE, Combs DM, Lechuga OM, Mader JJ, Udayasankaran J (2004) An Overview of Freeform Optics Production. *Proceedings of the SPIE* 5494.
[37] Dai YF, Guan CL, Yin ZQ (2010) Tool Decentration Effect in Slow Tool Servo Diamond Turning Off-axis Conic Aspheric Surface. *Proceedings of the SPIE* 7655.
[38] Dannberg P, Mann G, Wagner L, Brauer A (2000) Polymer UV-moulding for Micro-optical Systems and O/E-integration Micromachine Technology for Micro-optics. *Proceedings SPIE* 4179:137–145.
[39] Danzebrink HU, Koenders L, Wilkening G, Yacoot A, Kunzmann H (2006) Advances in Scanning Force Microscopy for Dimensional Metrology. *CIRP Annals – Manufacturing Technology* 55(2):841–879.
[40] Davis E, Roblee JW (2009) Comparison of Freeform Manufacturing Techniques in the Production of Monolithic Lens Arrays. *Proceedings of the SPIE* 7426:742605–742611.
[41] Davis GE, Roblee JW, Omecinski SM, Hedges (2010) A Comparison of Linear *Z*-axis and Rotational *B*-axis Freeform Diamond Turning in International Optical Design Conference and Optical Fabrication and Testing. *OSA Technical Digest (CD)* OTuD1. http://dx.doi.org/10.1364/OFT.2010.OTuD1.
[42] De Chiffre L, Kunzmann H, Peggs G, Lucca DA (2003) Surfaces in Precision Engineering, Microengineering and Nanotechnology. *CIRP Annals – Manufacturing Technology* 52(2):561–577.
[43] Ding Y, Liu X, Zheng ZR, Gu PF (2008) Freeform LED Lens for Uniform Illumination. *Optics Express* 16(17):12958–12966.
[44] Donker RL, Widdershoven I, Spaan HAM (2010) ISARA 400: Enabling Ultra-precision Coordinate Metrology for Large Parts. *Proceedings of the 10th International Euspen Conference*.
[45] Dörband B, Seitz G (2001) Interferometric Testing of Optical Surfaces at its Current Limit. *Optik* 112(9):392–398.
[46] Dowski ER, Cathey WT (1995) Extended Depth of Field Through Wave-front Coding. *Applied Optics* 34(11):1859–1866.
[47] Dumas PR, Fleig J, Forbes GW, Golini D, et al (2004) Flexible Polishing and Metrology Solutions for Free-form Optics. *Proceedings of the SPIE* 5494:39–44.
[48] Duparré JW, Wippermann FC (2006) Micro-optical Artificial Compound Eyes. *Bioinspiration & Biomimetics* 1:R1–R16.
[49] Elfizy AT, Bone GM, Elbestawi MA (2005) Design and Control of a Dual-stage Feed Drive. *International Journal of Machine Tools & Manufacture* 45(2):153–165.
[50] Evans CJ (2008) Uncertainty Evaluation for Measurements of Peak-to-valley Surface form Errors. *CIRP Annals – Manufacturing Technology* 57(1):509–512.
[51] Evans CJ (2010) Certification, Self-calibration, and Uncertainty in Testing Optical Flats. *Proceedings of the SPIE* 7656:76560S. http://dx.doi.org/10.1117/12.865762.
[52] Evans CJ, Bryan JB (1999) Structured, Textured or Engineered Surfaces. *CIRP Annals – Manufacturing Technology* 48(2):541–556.
[53] Evans CJ, Hocken RJ, Estler WT (1996) Self-calibration: Reversal, Redundancy, Error Separation and Absolute Testing. *CIRP Annals – Manufacturing Technology* 45(2):617–634.
[54] Fan KC, Fei YT, Yu XF, Chen YJ, Wang WL, Chen F, Liu YS (2006) Development of a Low-cost micro-CMM for 3D Micro/nano Measurements. *Measurement Science and Technology* 17(3):524–532.
[55] Fang FZ, Chen YH, Zhang XD, Hu XT, Zhang GX (2011) Nanometric Cutting of Single Crystal Silicon Surfaces Modified by Ion Implantation. *CIRP Annals – Manufacturing Technology* 60(1):527–530.
[56] Fang FZ, Liu YC (2004) On Minimum Exit-burr in Micro Cutting. *Journal of Micromechanics and Microengineering* 14:984–988.
[57] Fang FZ, Wu H, Liu YC (2005) Modeling and Investigation on Machining Mechanism of Nano-cutting Monocrystalline Silicon. *International Journal of Machine Tools and Manufacture* 45:1681–1686.
[58] Fang FZ, Wu H, Zhou W, Hu XT (2007) A Study on Mechanism of Nano-cutting Single Crystal Silicon. *Journal of Materials Processing Technology* 184(1–3):210–407.
[59] Fang FZ, Xiong Z, Hu XT (2006) An Experimental Study of Micromachining Step-mirror for Laser Diode Beam Shaping. *Journal of Micromechanics and Microengineering* 16:214–218.
[60] Fang FZ, Zhang XD, Hu XT (2008) Cylindrical Coordinate Machining of Optical Freeform Surface. *Optics Express* 16:7323–7329.
[61] Fang FZ, Venkatesh VC (1998) Diamond Cutting of Silicon with Nanometric Finish. *CIRP Annals – Manufacturing Technology* 47(1):45–49.
[62] Feng ZX, Luo Y, Han YJ (2010) Design of LED Freeform Optical System for Road Lighting with High Luminance/Illuminance Ratio. *Optics Express* 18(21):22020–22031.
[63] Flucke C, Gläbe R, Brinksmeier E (2008) Diamond Micro Chiselling of Molding Inserts for Optical Micro Structures. *Proceedings of the 23th ASPE Annual Meeting and 12th ICPE*, Portland.
[64] Forbes GW (2007) Shape Specification for Axially Symmetric Optical Surfaces. *Optics Express* 15(8):5218–5226.
[65] Forbes GW (2012) Characterizing the Shape of Freeform Optics. *Optics Express* 20(3):2483–2499.
[66] Fournier F, Rolland J (2008) Design Methodology for High Brightness Projectors. *Journal of Display Technology* 4:86–91.
[67] Fournier F, Rolland J (2008) Optimization of Freeform Lightpipes for Light-emitting-diode Projectors. *Applied Optics* 47:957–966.
[68] Gao F, Leach RK, Petzing J, Coupland JM (2008) Surface Measurement Errors Using Commercial Scanning White Light Interferometers. *MST 19 Id015303*.
[69] Gao W (2008) Fabrication of Large-area Micro-lens Arrays with Fast Tool Control. *International Journal of Precision Engineering and Manufacturing* 9(4):32–38.
[70] Gao W, Aoki J, Ju BF, Kiyono S (2007) Surface Profile Measurement of a Sinusoidal Grid Using an Atomic Force MICROScope on a Diamond Turning Machine. *Precision Engineering* 31:304–309.
[71] Gao W, Araki T, Kiyono S, Okazaki Y, Yamanaka M (2003) Precision Nano-fabrication and Evaluation of a Large Area Sinusoidal Grid Surface for a Surface Encoder. *Precision Engineering* 27:289–298.
[72] Garcia-Botella A, Fernandez-Balbuena AA, Bernabeu E (2006) Elliptical Concentrators. *Applied Optics* 45:7622–7627.
[73] Garrard K, Bruegge T, Hoffman J, Dow T, Sohn A (2005) Design Tools for Freeform Optics. *Proceedings of the SPIE* 5874:95–105.
[74] Geckeler RD, Just A (2007) Optimized Use and Calibration of Autocollimators in Deflectometry. *Proceedings of the SPIE* 6704:670407.1–670407.12.
[75] Gläbe R, Flucke C, Bothe T, Brinksmeier E (2005) High Speed Fringe Reflection Technique for nm Resolution Topometry of Diamond Turned Free Form Mirrors. *Proceedings of 5th euspen International Conference*.
[76] Gogotsi Y, Baek C, Kirscht F (1999) Raman Microspectroscopy Study of Processing-induced Phase Transformations and Residual Stress. *Semiconductor Science and Technology* 14:936–944.
[77] Gutierrez HM, Ro PI (2005) Magnetic Servo Levitation by Sliding-mode Control of Nonaffine Systems with Algebraic Input Invertibility. *IEEE Transactions on Industrial Electronics* 52(5):1449–1455.
[78] Haitjema H, Pril WO, Schellekens PHJ (2001) Development of a Silicon-based Nanoprobe System for 3-d Measurements. *CIRP Annals – Manufacturing Technology* 50(1):365–368.
[79] Hao X, Zheng ZR, Liu X, Gu PF (2008) Freeform Surface Lens Design for Uniform Illumination. *Journal of Optics A Pure and Applied Optics* 10(7):075005.
[80] Henselmans R (2009) *Non-contact measurement machine for freeform optics, Technische Universiteit Eindhoven*. (PhD thesis).
[81] Henselmans R, Cacace LA, Kramer GFY, Rosielle PCJN, et al (2011) The NANOMEFOS Non-contact Measurement Machine for Freeform Optics. *Precision Engineering* 35:607–624.
[82] Hicks RA (2007) Direct Methods for Freeform Surface Design. *Proceedings of the SPIE* 6668:666802.
[83] Hicks RA (2008) Controlling a Ray Bundle With a Free-form Reflector. *Optics Letters* 33:1672–1674.
[84] Hidaka K, Schellekens PHJ (2006) Study of a Small-sized Ultrasonic Probe. *CIRP Annals – Manufacturing Technology* 55(1):567–570.
[85] Horisaki R, Irie S, Ogura Y, Tanida J (2007) Three-dimensional Information Acquisition Using a Compound Imaging System. *Optical Review* 14(5):347–350.
[86] Hoshi H, Taniguchi N, Morishima H, et al (1996) *Off-axial HMD optical system consisting of aspherical surfaces without rotational symmetry SPIE*, vol. 3653. 234–242.
[87] Huang CN (2008) *Investigation of injection molding process for high precision polymer lens manufacturing*, The Ohio State University.
[88] Huang CN, Li L, Yi AY (2009) Design and Fabrication of a Micro Alvarez Lens Array with a Variable Focal Length. *Microsystem Technologies* 15:559–563.
[89] ISO/IEC Guide 99, 1993, International Vocabulary of Basic and General Terms in Metrology.
[90] ISO 13565-1, 1996, Geometrical product specification (GPS) – surface texture: profile method – profile method for surfaces having stratified functionalproperties. Part 1. Filtering and general measurement conditions.

[91] ISO 25178-2, 2012, Geometrical Product Specification (GPS) – Surface Texture: Areal – Part 2: Terms, Definitions and Surface Texture Parameters.
[92] ISO/TS 16610-29, 2006, Geometrical product specifications (GPS) – data extraction techniques by sampling and filtration – Part 29: Spline wavelets.
[93] ISO/TS 16610-31, 2010, Geometrical product specifications (GPS) – filtration – Part 31: Robust profile filters: Gaussian regression filter.
[94] ISO/TS 16610-32, 2009, 200Geometrical product specifications (GPS) – filtration – Part 32: Robust profile filters: Gaussian Regression Filter.
[95] ISO/TS 16610-40, 2006, Geometrical product specifications (GPS) – filtration – Part 40: Morphological profile filters: basic concept; 2002.
[96] ISO/TS 16610-41, 2006, Geometrical product specifications (GPS) – filtration – Part 41: Morphological profile filters: disk and horizontal seg-ment filters; 2002.
[97] ISO/TS 16610-49, 2006, Geometrical product specifications (GPS) – filtration – Part 49: Morphological profile filters: scale space techniques; 2002.
[98] ISO/WD 10110-19, 2006, Optics and photonics – preparation of drawings for optical elements and systems – Part 19: Freeform surfaces; 2012.
[99] ISO11562. *Geometrical Product Specification (GPS) – Surface Texture: Profile Method – Metrological Characteristics of Phase Correct Filters*, International Organization for Standardization, Geneva.
[100] Jäger G, Manske E, Hausotte T (2001) Nanopositioning and Measuring Machine. *Proceedings of 2nd Euspen International Conference*, 290–293.
[101] Jenkins D, Winston R (1996) Tailored Reflectors for Illumination. *Applied Optics* 35(10):1669–1672.
[102] Jiang X, Cooper P, Scott PJ (2010) Freeform Surface Filtering Using the Diffusion Equation. *Proceedings of the Royal Society A* 467:841–859.
[103] Jiang XJ, Scott PJ, WhiteHouse DJ (2007) Freeform Surface Characterisation – A Fresh Strategy. *CIRP Annals – Manufacturing Technology* 56(1):553–556.
[104] Jiang XJ, Scott PJ, Whitehouse DJ, Blunt L (2007) Paradigm Shifts in Surface Metrology. Part II. The Current Shift. *Proceedings of the Royal Society A* 463:2071–2099.
[105] Jiang XJ, Scott PJ, Whitehouse DJ, Blunt L (2007) Paradigm Shifts in Surface Metrology. Part I. Historical Philosophy. *Proceedings of the Royal Society A* 463:2049–2070.
[106] Jiang XJ, Whitehouse DJ (2012) Technological Shifts in Surface Metrology. *CIRP Annals – Manufacturing Technology* 61(2):815–836.
[107] Jones C (2012) *High Dynamic Range Surface Metrology*, Point measuring systems, euspen topical meeting: structure and freeform surfaces, Baden, Austria.
[108] Kanolt, C.W., 1959, Multifocal opthalmic lenses, United States Patent, 2 (878):721.
[109] Kapusi D, Machleidt T, Manske E, Franke KH, Jahn R (2008) White Light Interferometry Utilizing the Large Measuring Volume of a Nanopositioning and Nanomeasuring Machine. *Proceedings/International Colloquium on Surfaces (Chemnitz: 2008)*, Aachen Shaker, 210–217.
[110] Kase K, Makinouchi A, Nakagawa T, Suzuki H, Kimura F (1999) Shape Error Evaluation Method of Free-form Surfaces. *Computer-Aided Design* 31(8):495–505.
[111] Kaya I, Thompson KP, Rolland JP (2011) Edge Clustered Fitting Grids for (-Polynomial Characterization of Freeform Optical Surfaces. *Optics Express* 19(27):26962–26974.
[112] Kim S, Kang S (2003) Replication Qualities and Optical Properties of UV-moulded Microlens Arrays. *Jounral of Physics D Applied Physics* 36:2451–2456.
[113] Ko KH, Maekawa T, Patrikalakis NM (2003) An Algorithm for Optimal Free-form Object Matching. *Computer-Aided Design* 25:913–923.
[114] Ko KH, Maekawa T, Patrikalakis NM, Masuda H, Wolter FE (2003) Shape Intrinsic Properties for Free-form Object Matching. *Journal of Computing and Information Science in Engineering* 3:325–333.
[115] Kochengin S, Oliker V, Tempski OV (1998) On the Design of Reflectors with Prespecified Distribution of Virtual Sources and Intensities. *Inverse Problesms* 14:661–678.
[116] Komanduri RC, Raff LM (2001) Molecular Dynamics Simulation of the Nanometric Cutting of Silicon. *Philosophical Magazine B* 81(12):1989–2019.
[117] Kong LB, Cheung CF, To S, Lee WB (2009) An Investigation into Surface Generation in Ultra-precision Raster Milling. *Journal of Materials Processing Technology* 209(8):4178–4418.
[118] Kong LB, Cheung CF, To S, Lee WB, et al (2007) Measuring Optical Freeform Surfaces Using a Coupled Reference Data Method. *Measurement Science and Technology* 18:2252.
[119] Krishnasamy R, Wong W, Shen E, Pepic S, Hornsey R, Thomas PJ (2004) High Precision Target Tracking with a Compound-eye Image Sensor. *Proceedings of CCECE 2004-CCGEI 2004*, Niagara Falls.
[120] Kubala K, Dowski E, Cathey W (2003) Reducing Complexity in Computational Imaging Systems. *Optics Express* 11(18):2102–2108.
[121] Kunnavakkam MV, Houlihan FM, Schlax M, Liddle JA, et al (2003) Low-cost, Low-loss Microlens Arrays Fabricated by Soft-lithography Replication Process. *Applied Physics Letters* 82:1152–1154.
[122] Lai K, Rosenbluth AE, Bagheri S, et al (2009) Experimental Result and Simulation Analysis for the Use of Pixelated Illumination from Source Mask Optimization for 22 nm Logic Lithography Process. *Proceedings of the SPIE* 7274:72740A.
[123] Leach P (2012) *Surface metrology with nanometre accuracy: euspen topical meeting: structured and freeform surfaces*.
[124] Lee D, Haynes R, Ren D, et al (2001) Characterization of Lenslet Arrays for Astronomical Spectroscopy. *Paublication of the Astronomical Society of the Pacific* 113:1406–1419.
[125] Lee KW, Noh YJ, Arai Y, Shimizu Y, Gao W (2011) Precision mEasurement of Micro-lens Profile by Using a Force-controlled Diamond Cutting Tool on an Ultra-precision Lathe. *International Journal of Precision Technology* 2:211–225.
[126] Li G, Wang B, Dong S (2009) Design and Control of Dual-stage Feed Drive System in Ultra-precision Machine Tools. *Optics and Precision Engineering* 17(6):1426–1430.
[127] Li HF, Cheung CF, Jiang XQ, Lee WB, et al (2006) A Novel Robust Gaussian Filtering Method for the Characterization of Surface Generation in Ultra-precision Machining. *Precision Engineering* 30:421–430.
[128] Li L, Yi AY (2010) Design and Fabrication of a Freeform Prism Array for 3D Microscopy. *Journal of the Optical Society of America A* 27:2613–2620.
[129] Li L, Yi AY (2012) Design and Fabrication of a Freeform Microlens Array for a Compact Large-field-of-view Compound-eye Camera. *Applied Optics* 51:1843–1852.
[130] Li LK, Yi AY (2011) Design and Fabrication of a Freeform Microlens Array for Uniform Beam Shaping. *Microsystem Technologies* 17:1713–1720.
[131] Liebrich T, Knapp W (2012) Improvements and Experimental Validation of a 3D-probing System for Micro-components. *CIRP Annals – Manufacturing Technology* 61(1):475–478.
[132] Liu Q, Zhou XQ, Wang LD (2010) A New Hybrid Macro- and Micro-range Fast Tool Servo. *International Conference on Mechanic Automation and Control Engineering (MACE), 2010 International Conference on IEEE, vol. 2010*, 3124–3127.
[133] Liu YT, Li BJ (2010) Precision Positioning Device Using the Combined Piezo-VCM Actuator with Frictional Constraint. *Precision Engineering* 34(3):534–545.
[134] Liu YW (2000) Development of Huston's Method on Multi-body Dynamics. *China Mechanichal Engineering* 11(6):601–607.
[135] Lu XD, Trumper DL (2005) Ultrafast Tool Servos for Diamond Yurning. *CIRP Annals – Manufacturing Technology* 54(1):383–388.
[136] Luo Y, Feng ZX, Han YJ, Li HT (2010) Design of Compact and Smooth Free-form Optical System with Uniform Illuminance for LED Source. *Optics Express* 18(9):9055–9063.
[137] Ma T, Yu JC, Liang P, et al (2012) Design of a Freeform Varifocal Panoramic Optical System with Specified Annular Center of Field of View. *Optics Express* 19(5):3843–3853.
[138] Malacara D (2007) *Optical Shop Testing*, Wiley-Interscience. (ISBN 978-0-470135-96-9).
[139] Mallock A (1881) The Action of Cutting Tools. *Proceedings of the Royal Society of London* 33:127.
[140] Manske E, Hausotte T, Mastylo R, Machleidt T, Franke KH, Jäger G (2007) New Applications of the Nanopositioning and Nanomeasuring Machine by Using Advanced Tactile and Non-tactile Probes. *MST* 18:520–527.
[141] Marinello F, Bariani P, De Chiffer L, Savio E (2007) Fast Technique for AFM Vertical Drift Compensation. *Measurement Science & Technology* 18:689–696.
[142] Marinello F, Bariani P, Pasquini A, de Chiffre L, Bossard M, Picotto GB (2007) Increase of Maximum Detectable Slope with Optical Profilers, Through Controlled Tilting and Image Processing. *Measurement Science & Technology* 18:384–389.
[143] Marinello F, Savio E, Carmignato S, Bariani P, De Chiffre L, Bossard M (2007) Increase of Maximum Detectable Slope with Optical Profilers: Theory and Applicative Examples. *Proceedings of the 7th euspen, vol. 1*, 333–336.
[144] Marinello F, Bariani P, Pasquini A, de Chiffre L, et al (2007) Increase of Maximum Detectable Slope with Optical Profilers, Through Controlled Tilting and Image Processing. *Measurement Science & Technology* 18(2):384–389.
[145] Marks DL, Stack RA, Brady DJ (1999) Three-dimensional Tomography Using a Cubic-phase Plate Extended Depth-of-field System. *Optics Letters* 24(4):253–255.
[146] Memorandum to US Industrial Metrologists. (2007) Three Flat Method for Calibration of Optical Flats and ISO 17025. NIST press.
[147] Merchant ME (1944) Basic Mechanics of the Metal Cutting Process. *Journal of Applied Mechanics Review* A11:168–175.
[148] Mĩano JC, Benítez P, González JC (1995) RX, a Nonimaging Concentrator. *Applied Optics* 34:2226–2235.
[149] Michaeli W, Heßner S, Klaiber F, Forster J (2007) Geometrical Accuracy and Optical Performance of Injection Moulded and Injection-compression Moulded Plastic Parts. *CIRP Annals – Manufacturing Technology* 56(1):545–548.
[150] Millerd J, Brock N, Hayes J, North-Morris M, Novak M, Wyant JC (2004) Pixelated Phase-mask Dynamic Interfero-meter. *Proceedings of the SPIE* 5531:304–314.
[151] Miñano JC, Benítez P, Blen José (2008) High-efficiency Free-form Condenser Overcoming Rotational Symmetry Limitations. *Optics Express* 16:20193–20205.
[152] Miñano JC, Benitez P, Santamaria A (2009) Free-form Optics for Illumination. *Optical Review* 16:99.
[153] Miñano JC, Gonzáles JC (1992) New Method of Design of Nonimaging Concentrators. *Applied Optics* 31:3051–3060.
[154] Miñano JC, González JC, Benítez P (1995) A High-gain, Compact, Nonimaging Concentrator: RXI. *Applied Optics* 34:7850–7856.
[155] Miyashita T (2007) Standardization for Microlenses and Microlens Arrays. *Japanese Journal of Applied Physics* 46(8B):5391–5396.
[156] Mizutani K, Kawano T, Tanaka Y (1990) A Piezoelectric-drive Table and its Application to Micro-grinding of Ceramics Materials. *Precision Engineering* 12:219–226.
[157] Molly P, Schinker MG, Doell W (1987) Brittle Fracture Mechanisms in Single Point Glass Abrasion. *Proceedings of the SPIE* 802:81–88.
[158] Moreno I, Sun CC (2008) Modeling the Radiation Pattern of LEDs. *Optics Express* 16(3):1808.
[159] Morimoto Y, Ichida Y, Sato R, et al (2008) Development of Cutting Device with Enlargement Mechanism of Displacement – Application of Non-circular Cutting. *Journal of Advanced Mechanical Design Systems and Manufacturing* 2(4):474–481.
[160] Moriya T, Nakamoto K, Ishida T, Takeuchi Y (2010) Creation of V-shaped Microgrooves with Flat-ends by 6-axis Control Ultraprecision Machining. *CIRP Annals – Manufacturing Technology* 59(1):61–66.

[161] Moriyasu S, Yamagata Y, Ohmori H, et al., 2003, Probe type shape measuring sensor, and NC processing equipment and shape measuring method using the sensor, US Patent 6539642.

[162] Muñoz F, Benítez P, Miñano JC (2008) High-order Aspherics: The SMS Nonimaging Design Method Applied to Imaging Optics. *Proceedings of the SPIE 7061 70610G*. http://dx.doi.org/10.1117/12.794854.

[163] Noh YJ, Arai Y, Gao W (2009) Improvement of a Fast Tool Control Unit for Cutting Force Measurement in Diamond Turning of Micro-lens Array. *International Journal of Surface Science and Engineering* 3(3):227–241.

[164] Nussbaum P, Volkel R, Herzig HP, et al (1997) Design, Fabrication and Testing of Microlens Arrays for Sensors and Microsystems. *Pure and Applied Optics* 6:617–636.

[165] Ohl RG, Dow T, Sohn AA, et al (2004) Highlights of the ASPE 2004 Winter Topical Meeting on Free-form Optics: Design, Fabrication, Metrology, Assembly. *Proceedings of the SPIE* 5494:49–56.

[166] Ohmori H, Marinescu ID, Katahira K (2011) *Electrolytic In-Process Dressing (ELID) Technologies: Fundamentals and Applications*, CRC Press.

[167] Ohmori H, Watanabe Y, Lin WM, Katahira K, Suzuki T (2005) An Ultraprecision On-machine Measurement System. *Key Engineering Materials* 295/296:375–380.

[168] Oliker V (2005) Geometric and Variational Methods in Optical Design of Reflecting Surfaces with Prescribed Irradiance Properties. *Proceedings of the SPIE* 5924:592407.

[169] Oliker V (2006) Freeform Optical Systems with Prescribed Irradiance Properties in Near-Field. *Proceedings of the SPIE* 6342(2).

[170] Oliker V (2007) Optical Design of Freeform Two-mirror Beam-shaping Systems. *Journal of the Optical Society of America A* 24:3741–3752.

[171] Ong PT, Gordon JM, Rabl A (1996) Tailored Edge-ray Designs for Illumination with Tubular Source. *Applied Optics* 35(22):4321–4371.

[172] Osmer J, Weingärtner S, Riemer O, Brinksmeier E, et al (2007) Diamond Machining of Free-form Surfaces: A Comparison of Raster Milling and Slow Tool Servo Machining. *Proceedings of the 7th euspen International Conference*, 189–192.

[173] Ottevaere H, Volckaerts B, Lamprecht J, Schwider J, et al (2002) Two-dimensional Plastic Microlens Arrays by Deep Lithography with Protons: Fabrication and Characterization. *Journal of Optics A Pure and Applied Optics* 4(S22). http://dx.doi.org/10.1088/1464-4258/4/4/354.

[174] Owari H, Kawai S, Mukai Y, Terada S, et al (2006) Technology Development of Mold Fabrication for Free-form Surface, DOE and Microlens. *Proceedings of the SPIE* 6110:61100T.

[175] Parkyn B, Pelka D (2006) Free-form Illumination Lenses Designed by a Pseudo-rectangular Lawnmower Algorithm. *Proceedings of the SPIE* 6338:633803.

[176] Parkyn WA (1998) Design of Illumination Lenses Via Extrinsic Differential Geometry. *Proceedings of the SPIE* 3428:154–162.

[177] Parkyn WA, Gleckman PL, Pelka DG (1993) Converging TIR Lens for Non-imaging Concentration of Light From Compact Incoherent Sources. *Proceedings of the SPIE* 2016. http://dx.doi.org/10.1117/12.161947.

[178] Patterson SR, Magrab EB (1985) Design and Testing of a Fast Tool Servo for Diamond Turning. *Precision Engineering* 7(3):123–128.

[179] Peters J, Bryan JB, Estler WT, Evans C, et al (2001) Contribution of CIRP to the Development of Metrology and Surface Quality Evaluation During the Last Fifty Years. *CIRP Annals – Manufacturing Technology* 50(2):471–488.

[180] Petz M, Tutsch R, Christoph R, Andraes M, Hopp B (2012) Tactile – Optical Probes for Three-dimensional Microparts. *Measurement* 45:2288–2298.

[181] Plummer WT (2005) Free-form optical components in some early commercial products. *Proc Of SPIE* 5865:586509.

[182] Pollicove HM (1988) Survey of Present Lens Molding Techniques. *Proceedings of the SPIE* 896.

[183] Pulli K (1999) Multiview Registration for Large Data Sets. *Second International Conference on 3-D Imaging and Modeling*, 160–168.

[184] Rabl A, Gordon JM (1994) Reflector Design for Illumination with Extended Sources: The Basic Solutions. *Applied Optics* 33(25):6012–6021.

[185] Ravishankar S, Dutt HNV, Gurumoorthy B (2010) Automated Inspection of Aircraft Parts Using a Modified ICP Algorithm. *The International Journal of Advanced Manufacturing Technology* 46:227–236.

[186] Richter C, Kurz M, Knauer M, Faber Ch (2009) Machine-integrated Measurement of Specular Free-formed Surfaces Using Phase-measuring Deflectometry, vol. 6. *EUSPEN 2009*, San Sebastian, Spain, 21.

[187] Ries H, Muschaweck J (2002) Tailored Freeform Optical Surfaces. *Journal Optical Society of America* 19(3):590–595.

[188] Ries H, Rabl A (1994) Edge-ray Principle of Nonimaging Optics. *Journal Optical Society of America* 11(10):2627–2632.

[189] Rodgers JM, Thompson KP (2004) Benefits of Freeform Mirror Surfaces in Optical Design. *Proceedings of the SPIE* 5494(31):73–78.

[190] Saunders IJ, Ploeg L, Dorrepaal M, van Venrooy B (2005) Fabrication and Metrology of Freeform Aluminium Mirrors for the SCUBA-2 Instrument. *Proceedings of the SPIE* 5869.

[191] Savio E, de Chiffre L, Schmitt R (2007) Metrology of Freeform Shaped Parts. *CIRP Annals – Manufacturing Technology* 56(2):810–835.

[192] Savio E, Marinello F, Bariani P, Carmignato S (2007) Feature-oriented Measurement Strategy in Atomic Force Microscopy. *CIRP Annals – Manufacturing Technology* 56(1):557–560.

[193] Scheiding S, Gebhardt A, Eberhardt R, et al (2009) Micro Lens Array Milling on Large Wafers. *Optik & Photonik* 4(4):41–45.

[194] Scheiding S, Yi AY, Gebhardt A, et al (2011) Freeform Manufacturing of a Microoptical Lens Array on a Steep Curved Substrate by Use of a Voice Coil Fast Tool Servo. *Optics Express* 19(24):23938–23951.

[195] Schellekens P, Rosielle N, Vermeulen H, Vermeulen M, Wetzels S, Pril W (1998) Design for Precision: Current Status and Trends. *CIRP Annals – Manufacturing Technology* 47(2):557–586.

[196] Schinker MG (1991) Sub-surface Damage Mechanisms at High-speed Ductile Machining of Optical Glasses. *Journal of the International Society for Precision Engineering and Nanotechnology* 13(3):208–218.

[197] Schinker MG, Döll W (1987) Turning of Optical Glasses at Room Temperature. *Proceedings of the SPIE* 802:70–80.

[198] Schruben JS (1972) Formulation a Reflector-design Problem for a Lighting Fixture. *Journal of the Optical Society of America* 62:1498–1501.

[199] Schuler A, Weckenmann A, Hausotte T (2012) Enhanced Measurement of High Aspect Ratio Surfaces by Applied Sensor Tilting. *Proceedings of the 20th IMEKO World Congress Metrology for Green Growth"09. 14.09.2012*, Busan, Südkorea.

[200] Seeger S, Laboureux X (2000) *Feature Extraction and Registration – An Overview. Principles of 3D Image Analysis and Synthesis*, Academic Publishers, Boston, Dordrecht, London153–166.

[201] Shaw L, Weckenmann A (2011) Automatic Registration Method for Hybrid Optical Coordinate Measuring Technology. *CIRP Annals – Manufacturing Technology* 60(1):539–542.

[202] Sherif S, Cathey WT, Dowski ER (2004) Phase Plate to Extend the Depth of Field of Incoherent Hybrid Imaging Systems. *Applied Optics* 43(13):2709–2721.

[203] Shibuya AY, Yoshikawa Y, Gao W, Nagaike Y, et al (2010) A Spiral Scanning Probe System for Micro-aspheric Surface Profile Measurement. *International Journal of Advanced Manufacturing Technology* 46:845–862.

[204] Shore P, Cunningham C, DeBra D, Evans CJ, Gilmozzif R, Kunzmann H, et al (2010) Precision Engineering for Astronomy and Gravity Science. *CIRP Annals – Manufacturing Technology* 59(2):694–716.

[205] Shorey A, Kordonski W, Tricard M (2005) Deterministic Precision Finishing of Domes and Conformal Optics. *Proceedings of the SPIE* 5786:310–318.

[206] Smilie PJ, Suleski TJ (2011) Variable-diameter Refractive Beam Shaping with Freeform Optical Surfaces. *Optics Letters* 36(21):4170–4172.

[207] Spanò P (2008) Free-forms Optics Into Astronomical Use: The Case of an All-mirror Anamorphic Collimator. *Proceedings of the SPI* 7018:701840.

[208] Stack J (2009) Freeform DOEs Extend Optical Lithography. *Chip Design*.

[209] Su P, Wang Y, Burge JH, Kaznatcheev K, Idir M (2012) Non-null Full Field X-ray Mirror Metrology Using SCOTS: A Reflection Deflectometry Approach. *Optics Express* 20(11):12393–12407.

[210] Sun LW, Jin SZ, Cen SY (2009) Free-form Microlens for Illumination Applications. *Applied Optics* 48(29):5520–5527.

[211] Suzuki H, Kodera S, Maekawa S, Morita N, et al (1998) Study on Precision Grinding of Micro Aspherical Surface by Inclined Rotational Grinding. *Journal Japan Society for Precision Engineering* 64:619–623.

[212] Suzuki N, Yokoi H, Shamoto E (2011) Micro/nano Sculpturing of Hardened Steel by Controlling Vibration Amplitude in Elliptical Vibration Cutting. *Precision Engineering* 35:44–50.

[213] Swain MV (1979) Microfracture About Scratches in Brittle Solids. *Proceedings of the Royal Society* A366:575–597.

[214] Takahashi K (2011) Development of Ultrawide-angle Compact Camera Using Free-form Optics. *Optical Review* 18(1):55–59.

[215] Takeuchi H, Yosizumi K, Tsutsumi H (2004) Ultrahigh Accurate 3-D Profilometer Using Atomic Force Probe of Measuring Nanometer. *Proceedings of ASPE Winter Topical Meeting*, 102–107.

[216] Takeuchi Y, Maeda S, Kawai T, Sawada K (2002) Manufacture of Multiple-focus Micro Fresnel Lenses by Means of Nonrotational Diamond Grooving. *CIRP Annals – Manufacturing Technology* 51(1):343–346.

[217] Takeuchi Y, Yoneyama Y, Ishida T, Kawai T (2009) 6-Axis Control Ultraprecision Microgrooving on Sculptured Surfaces with Non-rotational Cutting Tool. *CIRP Annals – Manufacturing Technology* 58(1):53–56.

[218] Tanigami M, Ogata S, Aoyama S, Yamashita T, Imanaka K (1989) Low Wavefront Aberration and High-temperature Stability Molded Micro Fresnel Lens. *Photonics Technology Letters IEEE* 1:384–385.

[219] Taniguchi N (1983) Current Status in and Future Trends of Ultraprecision Machining and Ultrafine Materials Processing. *CIRP Annals – Manufacturing Technology* 32(2):573–582.

[220] Timinger AL, Muscaweek JA, Ries H (2003) Designing Tailored Free-form Surfaces for General Illumination. *Proceedings of the SPIE* 5186:128–132.

[221] Toh SB, McPherson R (1986) Fine Scale Abrasive Wear of Ceramics by a Plastic Cutting Process, Science of Hard Materials. *Institute Physics Conference Series* 75(9):856–871.

[222] Tohme Y (2004) Slow Slide Servo (S3) machining of freeform optics – abstract. *Moore Nanotechnology Systems*. http://www.nanotechsys.com/technology/technical-papers/.

[223] Tohme Y (2007) Grinding Aspheric and Freeform Micro-optical Molds, Micromachining Technology for Micro-optics and Nano-optics. *Proceedings of the SPIE* 6462. (64620 K.1–64620 K.8).

[224] Tohme Y (2008) Trends in Ultra-precision Machining of Freeform Optical Surfaces. *Optical Fabrication and Testing OSA Technical Digest (CD) OThC6*.

[225] Trumper DL, Lu XD (2005) Electromagnetically-driven ultra-fast tool servos for diamond turning. PhD Dissertation. *Massachusetts Institute of Technology*.

[226] Uhlmann E, Häusler G, Kurz M, Faber Ch, et al (2011) Phase Measuring Deflectometry Setup for Machine Integrated Measurement of Specular Surfaces, vol. 2.49. *EUSPEN 2011*, Como, Italy.

[227] van den Berg R (2005) Extreme UV Lithography Preserves Moore's Law. *Optics & Laser Europe* 129:29–31.

[228] Walker DD, Beaucamp ATH, Doubrovski V, Dunn C, et al (2005) New Results Extending the Precessions Process to Smoothing Ground Aspheres and Producing Freeform Parts. *Proceedings of the SPIE* 5869:58690E. http://dx.doi.org/10.1117/12.617067.

[229] Wang K, Chen F, Liu ZY, Luo XB, et al (2010) Design of Compact Freeform Lens for Application Specific Light-emitting Diode Packaging. *Optics Express* 18(2):413–425.

[230] Wang K, Wu D, Chen F, Liu Z, et al (2010) Angular Color Uniformity Enhancement of White Light Emitting Diodes Integrated with Freeform Lenses. *Optics Letters* 35:1860–1862.
[231] Wang QC, Zhang XD, Peng Y, Fang FZ (2012) Data Filtering of Optical Freeform Measurement Based on a Modified 2D Cascaded Approximating Spline Filter. *Proceedings of the SPIE 8416 84160J*. http://dx.doi.org/10.1117/12.978166.
[232] Wang YB, Wang CL, Xing QR, Liu F, et al (2009) Periodic Optical Delay Line Based on a Tilted Parabolic Generatrix Helicoid Reflective Mirror. *Applied Optics* 48(11):1998–2005.
[233] Weckenmann A, Estler T, Peggs G, McMurtry D (2004) Probing Systems in Dimensional Metrology. *CIRP Annals – Manufacturing Technology* 53(2):657–684.
[234] Weckenmann A, Gawande B (1987) Prüfen von Werkstücken mit gekrümmten Flächen auf Koordinatenmessgeräten. *Technisches Messen tm* 54(7/8):277–284.
[235] Weckenmann A, Jiang X, Sommer KD, et al (2009) Multisensor Data Fusion in Dimensional Metrology. *CIRP Annals – Manufacturing Technology* 58(2):701–721.
[236] Weckenmann A, Peggs G, Hoffmann J (2006) Probing Systems for Dimensional Micro and Nano Metrology. *Measurement Science & Technology* 17(3):504–509.
[237] Weckenmann A, Peters RD (1983) Mathematische Beschreibung von gekrümmten Oberflächen für die Anwendung in der Koordinatenmesstechnik. *CIRP Annals – Manufacturing Technology* 32(1):453–457.
[238] Weckenmann A, Schuler A (2011) Application of Modern High Resolution Tactile Sensors for Micro-objects. *International Journal of Precision Technology* 2/2/3:266–288.
[239] Weckenmann A, Schuler A, Ngassam RJB (2011) enhanced Measurement of Steep Surfaces by Sensor Tilting. *Proceedings of the 56th international scientific colloquium, vol. ID 134*, Ilmenau, 1.
[240] Whitehouse DJ (1994) *Handbook of Surface Metrology*, Institute of Physics, Bristol. (ISBN 0-7503-0039-6).
[241] Widdershoven I, Donker RL, Spaan HAM (2011) Realization and Calibration of the Isara 400 Ultra-precision. *CMM Journal of Physics Conference Series* 311:012002.
[242] Winston R, Miñano JC, Benítez P (2005) *Nonimaging Optics*, Elsevier.
[243] Wu RM, Li HF, Zheng ZR, Liu X (2011) Freeform Lens Arrays For Off-axis Illumination in an Optical Lithography System. *Applied Optics* 50(5):725–732.
[244] Wyant JC (2003) Dynamic Interferometry. *Optics & Photonics News* 14(4):36–41.
[245] Wyant JC, Creath K (1992) *Basic Wavefront Aberration Theory for Optical Metrology Chapter 1 in Applied Optics and Optical Engineering*, XlAcademic Press. 28–39. 1992.
[246] Xu L, Chen K, He Q, Jin G (2009) Design of Freeform Mirrors in Czerny–Turner Spectrometers to Suppress Astigmatism. *Applied Optics* 48:2871–2879.
[247] Yabe A (2012) Representation of Freeform Surfaces Suitable for Optimization. *Applied Optics* 51(15):3054–3058.
[248] Yamamoto Y, Suzuki H, Okino T, Hijikata Y, Moriwaki T, et al (2004) Ultra Precision Grinding of Micro Aspherical Surface. *Proceedings of ASPE Annual Meeting*, 558–661.
[249] Yan JW, Asami T, Harada H (2009) Fundamental Investigation of Subsurface Damage in Single Crystalline Silicon Caused by Diamond Machining. *Precision Engineering* 33:378–386.
[250] Yan JW, Zhang ZY, Kuriyagawa T, Gonda H (2010) Fabricating Micro-structured Surface by Using Single-crystalline Diamond Endmill. *International Journal of Advanced Manufacturing Technology* 51:957–964.
[251] Yan JW, Zhao HW, Kuriyagawa T (2009) Effects of Tool Edge Radius on Ductile Machining of Silicon: An Investigation by FEM. *Semiconductor Science and Technology* 24:075018.
[252] Yashchuk VV, Barber S, Domning EE, Kirschman JL, et al (2010) Sub-microradian Surface Slope Metrology with the ALS Developmental Long Trace Profiler. *Nuclear Instruments and Methods in Physics Research A* 616(2/3):212–223.
[253] Yi AY, Li L (2005) Design and Fabrication of a Freeform Phase Plate for High-order Ocular Aberration Correction. *Applied Optics* 44(32):6869–6876.
[254] Yi AY, Li L (2005) Design and Fabrication of a Micro-lens Array by Use of a Slow Tool Servo. *Optics Letters* 30(13):1707–1709.
[255] Yin ZQ, Dai YF, Li SY (2011) Fabrication of Off-axis Aspheric Surfaces Using a Slow Tool Servo. *International Journal of Machine Tools & Manufacture* 51:404–410.
[256] Zamora P, Cvetkovic A, Buljan M, Hernandez M, et al (2009) Advanced PV Concentrators. *34th IEEE of Photovoltaic Specialists Conference*, 929–932.
[257] Zhang XD, Fang FZ, Wang HB, Wei GS, et al (2009) Ultra-precision Machining of Sinusoidal Surfaces Using the Cylindrical Coordinate Method. *Journal Micromechanics and Mircoengineering* 19:054004. (pp. 7).
[258] Zhang XD, Fang FZ, Wu QQ, Liu XL, Gao HM (2012) Coordinate Transformation Machining of Off-axis Aspheric Mirrors. *International Journal of Advanced Manufacturing Technology*. http://dx.doi.org/10.1007/s00170-012-4642-x.
[259] Zhang XD, Fang FZ, Yu LH, Jiang LL, Guo YW (2013) Slow Slide Servo Turning of Compound Eye Lens. *Optical Engineering* 52(2):023401.
[260] Zhang XD, Gao HM, Guo YW, Zhang GX (2012) Machining of Optical Freeform Prisms by Rotating Tools Turning. *CIRP Annals – Manufacturing Technology* 61(1):519–522.